KfK 4890
September 1991

Comparison of Turbulence Parameters Measured by SODAR and Sonic Anemometer

H. Gentou, P. Thomas, S. Vogt
Institut für Meteorologie und Klimaforschung

Kernforschungszentrum Karlsruhe

KERNFORSCHUNGSZENTRUM KARLSRUHE
Institut für Meteorologie und Klimaforschung

KfK 4890

Comparison of Turbulence Parameters Measured by SODAR and Sonic Anemometer

H. Gentou *, P. Thomas and S. Vogt

* delegated from Remtech S.A., 2 and 4, avenue de l'Europe, B.P. 159 - 78143 Vélizy Cedex - France.

Kernforschungszentrum Karlsruhe GmbH, Karlsruhe

Kernforschungszentrum Karlsruhe GmbH
Postfach 3640, 7500 Karlsruhe 1

ISSN 0303-4003

Abstract

A monostatic Doppler–SODAR and a sonic anemometer have been operated during June and July 1990 at the Nuclear Research Center Karlsruhe to measure 30 min mean values of the vertical wind speed and its standard deviation at 100 m above ground level. Other meteorological parameters have been additionally measured by the SODAR and at a 200 m high tower. During seven runs lasting about two hours each and covering different atmospheric stability conditions, instantaneous values of the vertical wind speed have been measured by both instruments, too, from which logarithmic power spectra have been calculated. From these spectra, the logarithmic spectral peak, the corresponding outer turbulent scale wavelength, and the integral scale of turbulence have been determined.

The longterm comparison of the standard deviation measured by both instruments was quantified by the bias, the root mean square error, the precision, and the correlation coefficient. The agreement of the data sets varies as a function of horizontal wind speed and atmospheric stability. In general, there is a better agreement during low wind situations and during nighttime. The SODAR is underestimating high values of the standard deviation.

The power spectra yielded by both instruments are generally well comparable in all atmospheric stability conditions. In particular, the logarithmic spectral peaks derived from SODAR and sonic data are almost coincident. During windy conditions, the inertial subrange slope of the SODAR spectra is not detailed and the definition of the spectral peak is difficult. In some cases, the spectra derived from SODAR data are underestimated.

Mit SODAR und Ultraschallanemometer gemessene Turbulenzparameter. Ein Vergleich

Zusammenfassung

Im Juni und Juli 1990 wurden am Kernforschungszentrum Karlsruhe mit einem monostatischen Doppler-SODAR und einem Ultraschallanemometer 30 min Mittelwerte des Vertikalwindes und der zugehörigen Standardabweichung in 100 m über Grund gemessen. Begleitend wurden andere meteorologische Größen mit dem SODAR und an einem 200 m hohen Mast bestimmt. Während sieben etwa zweistündigen Intervallen mit unterschiedlichen atmosphärischen Stabilitätsbedingungen wurden mit beiden Instrumenten zusätzlich Momentanwerte des Vertikalwindes gemessen und daraus Spektren berechnet. Aus diesem Spektren wurden Betrag und Frequenz des Maximum sowie die zugehörige sogenannte "outer turbulent scale

wavelength" bestimmt. Dieser Parameter charakterisiert die Größe der Turbulenzelemente in diesem Trägheitsunterbereich. Weiterhin wurde aus den Spektren der sogenannte "integral scale" der Turbulenz abgeleitet, der ein Maß für den zeitlichen Abfall der Autokorrelationsfunktion ist.

Für einen Langzeitvergleich der mit beiden Geräten gemessenen Standardabweichung des Vertikalwindes dienen die systematische Abweichung der Mittelwerte (Bias), die Wurzel der mittleren quadratischen Differenzen der jeweiligen Meßwerte (RMSE), und die Wurzel der mittleren quadratischen Differenzen der Abweichung der jeweiligen Meßwerte von ihrem Mittelwert (Precision) sowie der Korrelationskoeffizient. Die Übereinstimmung der beiden Datensätze variiert mit der horizontalen Windgeschwindigkeit und den atmosphärischen Stabilitätsbedingungen. Im allgemeinen ist die Übereinstimmungen gut, besonder während der Nacht. Das SODAR unterschätzt allerdings hohe Werte der Standardabweichung und während Zeiten hoher horizontaler Windgeschwindigkeit.

Die mit Hilfe beider Instrumente gewonnenen Spektren stimmen allgemein während aller atmosphärischen Stabilitätsbedingungen gut überein. Das gilt besonders für Betrag und Frequenz des Maximums. Während Zeiten hoher horizontaler Windgeschwindigkeit ist allerdings der hochfrequente Abfall der SODAR-Spektren im Trägheitunterbereich nur andeutungsweise vorhanden und damit die Bestimmung des Maximums schwierig. In einigen Fällen liefert das SODAR insgesamt zu niedrige Spektralwerte.

Contents

List of Figures

List of Tables

1 Introduction

Knowledge of the nature of turbulence in the atmospheric boundary layer is of great importance in many practical problems faced by atmospheric scientists. Recently, with the growing needs of air quality studies and pollution control, interest has increased in the capability of Doppler SODARs to measure turbulence parameters.

Determinations of the spectra of the vertical wind velocity w measured by a SODAR in the boundary layer are not plentiful. Asimakopoulos *et al.* (1978) presented the first intercomparison with *in situ* measurements. Congeduti *et al.* (1981) have shown that SODARs have the capability to determine vertical velocity spectra for frequencies up to $1/80$ Hz. Underwood and Coulter (1983) published a study of SODAR spectra which shows that in some atmospheric conditions, the peaks of logarithmic spectra derived from SODAR data are relatively well defined. Kaimal *et al.* (1984) compared commercially available Doppler SODAR with sonic anemometers and computed spectra of vertical velocity obtained by SODAR. But their main purpose was to explain the underestimation of the standard deviation σ_w measured by a SODAR due to the spatial averaging. Helmis *et al.* (1985) used a small high frequency SODAR to determine atmospheric turbulence parameters and spectra at low altitudes.

During the summer of 1990, a field test program was conducted by the Institut für Meteorologie und Klimaforschung (IMK) at the site of the Kernforschungszentrum-Karlsruhe (KfK) to evaluate the capabilities of SODARs to determine turbulence parameters. As the vertical wind velocity is very important to quantify atmospheric turbulence, it was simultaneously measured by the IMK-SODAR (type A0-REMTECH) and a sonic anemometer mounted at the 100 meter height level of the meteorological tower at KfK. The field experiment and the evaluation were split into two parts: a long term intercomparison of half hour mean values and a comparison of the measured spectra of the vertical wind velocity during seven short time periods (1.2 to 2.3 hours) covering all stability conditions.

The more general objectives of this experiment were (i) to collect sufficient samples of data for statistical and spectral analysis, (ii) to check the performance of the SODAR to determine turbulence parameters and (iii) to obtain information about the capability of SODAR to measure other turbulence parameters, such as $\overline{u'w'}$ or the scales of turbulence derived from spectra. Such features are useful as input data for numerical atmospheric models.

2 Instrumentation

2.1 SODAR

The monostatic three dimensional Doppler SODAR A0 is manufactured by the French enterprise REMTECH, with general characteristics listed in Table 1.

Table 1: General characteristics of the A0 Doppler-SODAR.

Centered frequency	around 1600 Hz
Acoustic transmitted power	60 W
3 dB beam width of antenna	$\pm$ 7°
Angle tilted antenna	18°
Pulse length	6 – 400 ms
Pulse repetition	0 to 20 s
Minimum height resolution	20 m
Number of range gates	20

The system uses a trailer mounted array of three antennae with two antennae tilted from the vertical to measure horizontal components of the wind vector. The SODAR emits a double frequency pulse of 150 ms duration with a centered frequency of 1600 Hz. Analysis of the backscattered echo using FFT was automatically done by the SODAR software. The rejection by software of backscattered echos was mainly due to fixed echos and ambient noise. Furthermore, after each 3 h a "big" calibration is automatically performed to take care of temperature variations.

2.1.1 Averaging mode

During the first part of the experiment (from 1 Juni 1990 to 31 July 1990), the SODAR measured wind data between 60 and 420 m above ground level (AGL) with a 20 m height resolution and a 4 to 5 s pulse repetition interval.

The SODAR adjusts for ambient noise variations with a 9 s small calibration after each 14 pulses, which, in this configuration, is at an interval of about 1 min. The averaging time interval chosen was 30 min, and the SODAR system stored the following parameters on magnetic device: backscattered echo intensity, horizontal (U) and vertical (w) wind speed, direction (θ), and standard deviations σ_w and σ_θ of vertical wind speed and direction.

2.1.2 Instantaneous mode

In the second part of the experiment, we chose the three measurement levels 80 m, 100 m and 120 m AGL, with a 20 m height resolution. Although it would have been possible to measure the three components of the wind vector, we used only the vertical antenna in order to obtain a short sampling interval which, in this configuration, was about 1.3 s. The date and time of the measuring periods are listed in Table 4.

Three problems appeared:

(i) The experimental site has a high environmental noise level and many fixed echos. So, even if there was a backscattered echo, the SODAR often rejected it.

(ii) It is not possible to suppress the small and big calibrations in the SODAR measuring cycle. The consequence is that the SODAR was measured for 18 s, then the transmission was stopped for about 9 s. The effects of this 27 s cycle on the time series are described in Appendices B and C.

(iii) Spectral analysis of data with randomly missing observations is not possible using classical methods. However, in Section 4 and Appendix A a new procedure that was recently developed by mathematicians is described to overcome this problem.

2.2 Sonic anemometer

The sonic anemometer-thermometer is a KAIJO DENKI model DAT 300 mounted on the meteorological tower at 100 m AGL. The probe model TR 61 C measures in three orthogonal directions. The distance between transducers is 20 cm. A detailed description of this instrument has been published by Hanufusa *et al.* (1982). General characteristics are given in Table 2. The sonic anemometer interface unit was linked to a computer through an RS 232 port. In the averaging mode, u, v, w, T, σ_w, $\overline{u'w'}$ and other parameters were stored every 10 min. In the instantaneous mode, the sampling interval was 1.06 s and only the components u, v, and w of the wind speed and the temperature T were available. No correction to compensate for the effects of wind shadowing by the transducers has been performed.

Table 2: General characteristics of the sonic anemometer-thermometer.

Internal sampling frequency	20 Hz
Path length (TR 61 C)	200 mm
Diameter of transducers	15 mm
Separation between axes	90°
Velocity resolution	0.01 ms^{-1}
Temperature resolution	0.025 $°C$

2.3 Site installation

The KfK tower is located in the Rhine valley about 4 km east from the river, and the local topography is roughly flat. Hills of a relative height of 200 and 500 m are situated repectively 8 km east and 30 km west of the Research Center. The wind blows predominently parallel to the valley direction, from south-west to north-east.

The KfK tower is an open lattice-type structure of square cross section with a side length of 1.5 m. The boom of the sonic anemometer is fixed at a height of 100 m on the north side and extended 4 m from the north-west tower corner. Seen from the centre of the tower, the direction of the sonic anemometer is $\approx 275°$ west, following meteorological conventions. Thus, the sonic anemometer is considered to be in the wind shadow when the wind comes from a direction between 70° and 120°.

The tower bears instruments at 10 levels, namely 20, 30, 40, 50, 60, 80, 100, 130, 160, and 200 m AGL, with cup-anemometers, temperature sensors, windvanes, and propvanes (Dilger (1976), von Holleuffer-Kypke *et al.* (1984)). These sensors were used to determine the atmospheric conditions during the experiments.

The SODAR was installed in a clearing (60 m $\times$ 100 m) of a pine forest, which surrounds the site. The average height of the pines in this area is about 20 m.

Figure 1 illustrates the position of the tower and the SODAR. It will be shown in Section 5 that the distance between the two instruments is too great to permit a direct comparison of vertical wind speed.

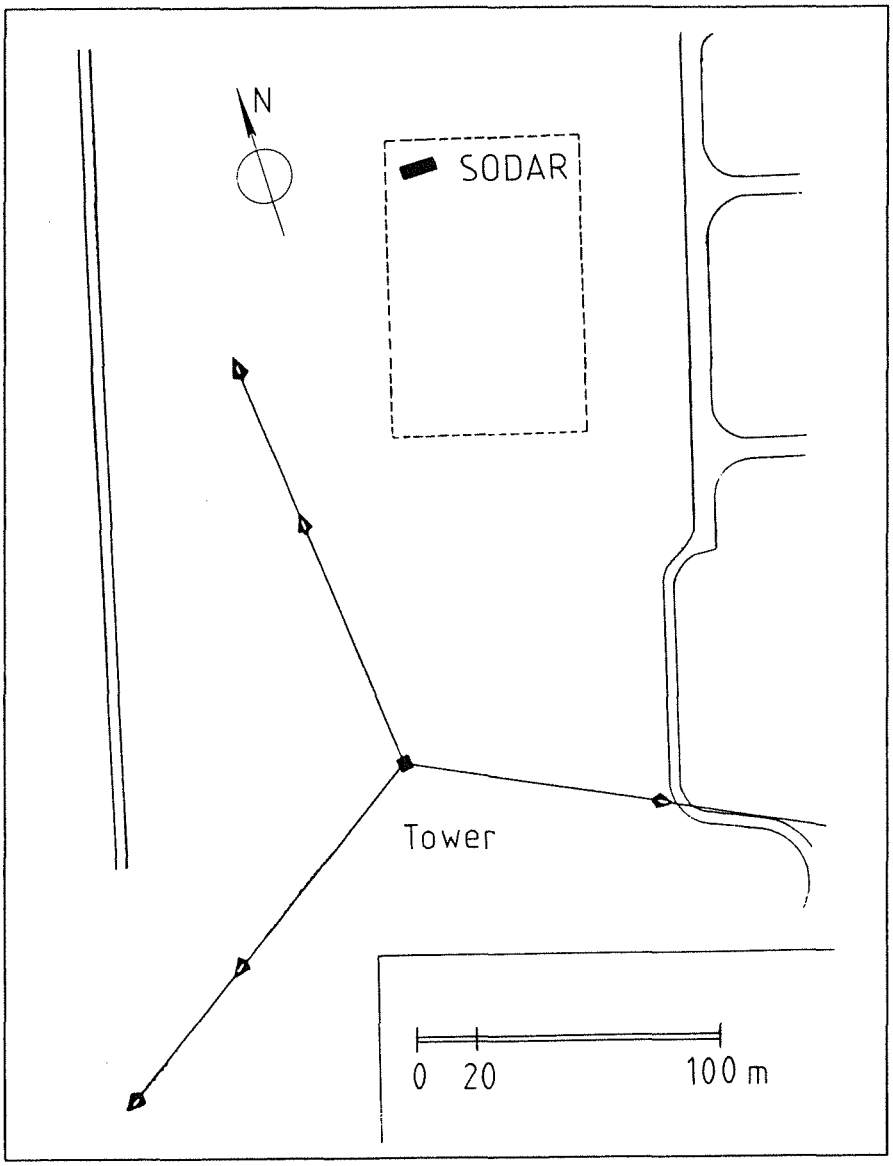

Figure 1: Plan of the experimental site.

3 Long term comparison

3.1 Analysis of mean values

The SODAR σ_w (Y_i) are compared to the sonic σ_w (X_i; averaged over 30 min) using data recorded during the months of June and July 1990. We have chosen to examine the four criteria:

$$B = \frac{1}{N}\sum_{i=1}^{N}\left(Y_i - X_i\right) \quad (1)$$

$$RMSE = \left[\frac{1}{N}\sum_{i=1}^{N}(Y_i - X_i)^2\right]^{1/2} \quad (2)$$

$$P = \left(RMSE^2 - B^2\right)^{1/2} \quad (3)$$

$$RP = \frac{P}{\bar{X}} \times 100 \quad (4)$$

with $\bar{X}$, being the mean of the sonic data, and N the number of data couples. These basic criteria, bias B, root mean square error $RMSE$, precision P, and relative precision RP are adopted from the study of SODARs conducted for the U.S. EPA by NOAA/ERL (Kaimal *et al.* (1984)). This means that the results of our investigation are comparable with previous studies (Kaimal *et al.* (1984), Chintawongvanich *et al.* (1989), Thomas and Vogt (1990)). Regression analysis of the data gives additional information about the linear relationship between X_i and Y_i. The relationship may be expressed as:

$$Y_i = aX_i + b + e_i \quad (5)$$

with

a : slope of the regression line

b : Y intercept of the regression line

e_i : error term

and the correlation coefficient is R.

3.2 Results of the comparison

This section focuses on some results and implications of our comparison between the mean values and compares them with those of SODAR measurement error models. Table 3 illustrates the results including the cases of wind shadow. Examination of the horizontal wind speed when the tower is upwind indicates calm conditions. As will be explained in this section, the measurement accuracy is better in calm conditions so the effect of wind shadow is comparatively small.

Table 3: Comparison of σ_w measured by SODAR and sonic during June and July, 1990.

	Day and night	Daytime	Nighttime
N	1509	857	536
$\bar{X}(ms^{-1})$	0.58	0.75	0.36
$\bar{Y}(ms^{-1})$	0.47	0.59	0.29
$B(ms^{-1})$	-0.12	-0.16	-0.07
RMSE (ms^{-1})	0.22	0.26	0.14
P (ms^{-1})	0.18	0.20	0.12
RP (%)	31.3	28.0	33.3
a	0.63	0.51	0.61
b (ms^{-1})	0.10	0.22	0.07
R	0.82	0.65	0.84

3.2.1 Influence of wind speed

Figures 2 and 3 depict plots of SODAR σ_w, sonic σ_w and the σ_w difference against the sonic horizontal wind speed U. Only every second data couple are plotted in the figures. It can be seen in Figure 2 that the SODAR measures accurately σ_w in the range zero to 0.4 ms^{-1}. This is partly possible with the help of the SODAR multifrequency signal. The SODAR interpretes the frequency difference of each backscattered echo analysed at the same time. Such method permits to reduce the error in measurement, especially at low wind speeds which can be confounded with fixed echos.

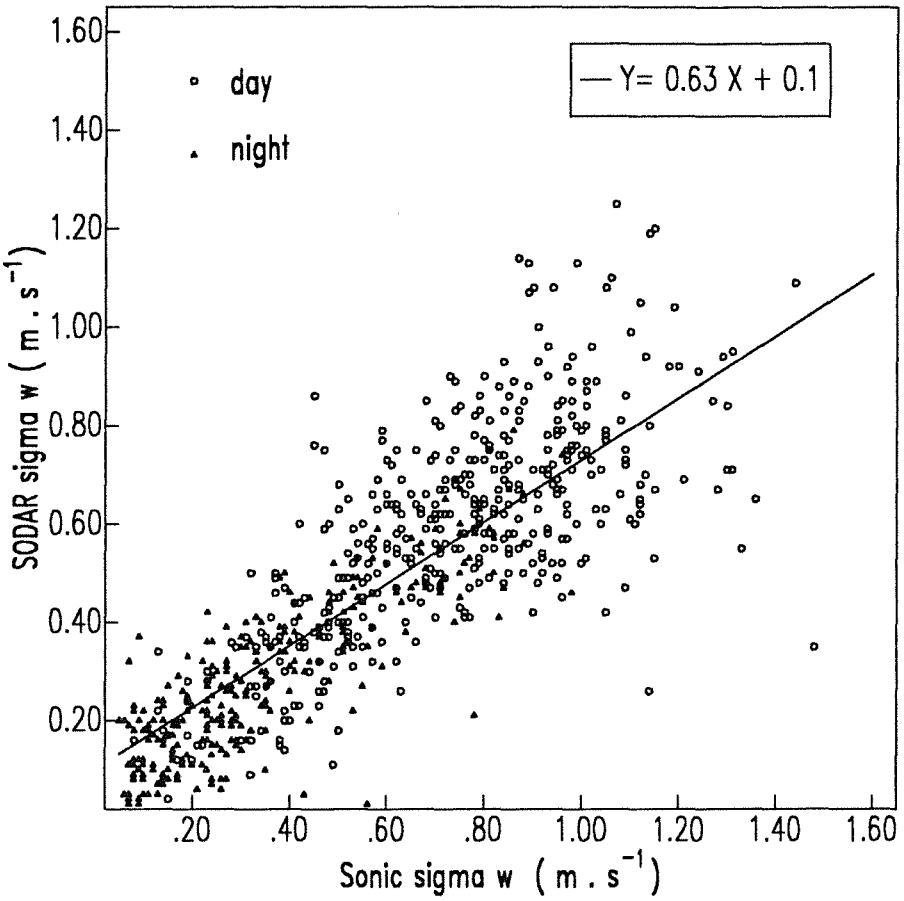

Figure 2: SODAR σ_w versus sonic σ_w measured at 100 m.

Figure 3 illustrates clearly that the SODAR σ_w measurement is not very accurate in windy conditions. In calm to medium conditions ($U \leq 6\ ms^{-1}$), the difference between the two measurements of σ_w is small, but the SODAR gradually underestimates σ_w with increasing horizontal wind speed.

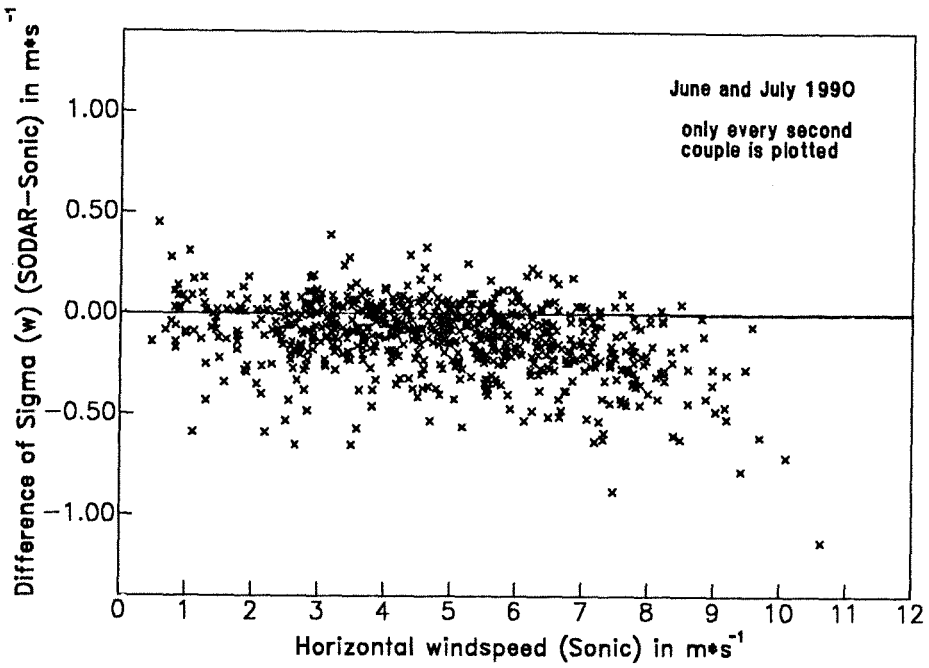

Figure 3: σ_w difference versus sonic horizontal wind speed measured at 100 m AGL.

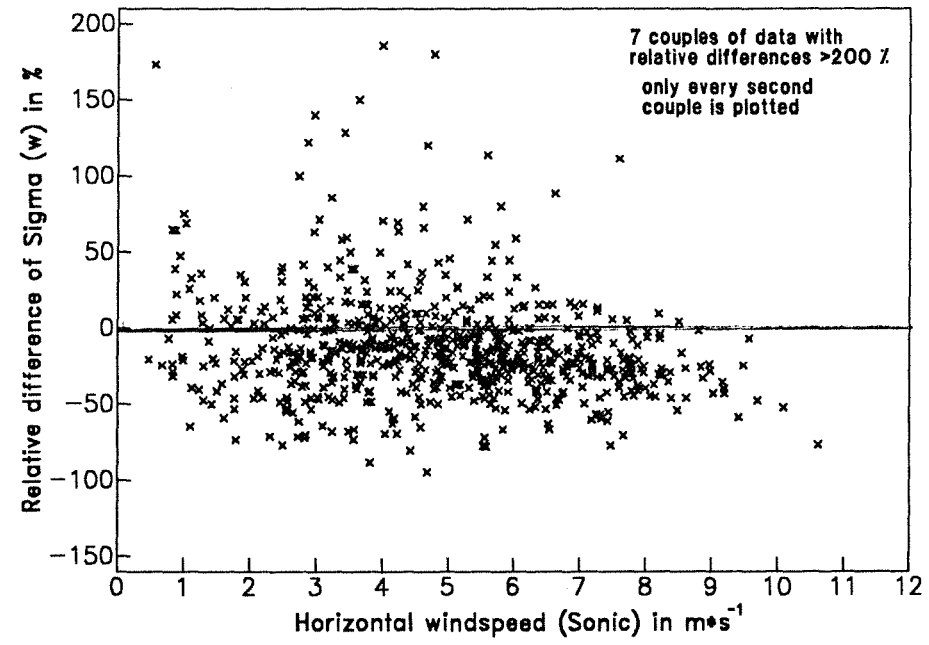

Figure 4: Relative difference $(\sigma_w^{SODAR} - \sigma_w^{sonic})/\sigma_w^{sonic}$ versus sonic horizontal wind speed measured at 100 m AGL.

The relative difference as a percentage illustrated in Figure 4 is low for windy conditions . Thus, even if the numerical difference between SODAR and sonic σ_w is greater in windy conditions, it is satisfying to see that the relative difference decreases with increasing horizontal wind speeds.

3.2.2 Influence of daytime and nighttime

We have differentiated the data into the categories daytime and nighttime (07h00 to 19h30 and 21h00 to 05h30 Central European Time - CET). During June and July 1990, the weather was mainly influenced by high pressure systems. This resulted in unstable atmospheric conditions during the day whereas stable conditions were prevalent during the night.

Table 3 indicates that the SODAR and the sonic anemometer are much better correlated at night than during the day. This suggests that the SODAR σ_w values are more accurate during calm and stable conditions than during windy and unstable conditions.

It should be noted that Kaimal *et al.* (1984), and Chintawongvanich *et al.* (1989) found similar results. The latter suggested that the poorer daytime results may be due to spatial inhomogeneity resulting from convection. In addition, they also suggested that the presence of gravity waves during the night may have contributed to better nighttime results.

3.3 Conclusions

Our study shows that the comparability of SODAR and sonic data varies, among other possible factors, with the horizontal wind speed and the atmospheric stability. The influence of wind speed is easily explained. As described in Appendix A, the area between two values of frequencies and the spectral density function is equal to the variance or covariance produced between the two frequencies involved. The total area represents the variance σ_w^2. Because of its low sampling rate, the SODAR is not able to measure the smallest fluctuations, those corresponding to a small part of the power. However, in windy conditions, the whole spectrum is shifted to higher frequencies and a greater part of the power is then filtered by the SODAR. This leads to a greater underestimation of the variance σ_w^2.

Kaimal *et al.* (1984) have studied the influence of aliasing and other factors on the vertical wind speed variance. Their study suggested that half the power above the Nyquist frequency n_o is aliased back. The other half would represent the variance loss through spatial averaging. Their conclusion was that a possible reason for the SODAR underestimation is the spatial averaging. However, they did not separate cases into windy and calm conditions.

Kristensen and Gaynor (1986) have published a study which presents a theoretical description and resulting applications of the effects of spatial

and temporal separation, and of volume sampling. In the case of σ_w measurements, spatial and temporal separation have no effect because only the vertical antenna is involved. In contrast, volume sampling does have an effect. They propose a correction of SODAR σ_w which involves knowledge of the integral scale of turbulence Λ (see Section 4.2.3):

$$\frac{\sigma^2}{\sigma_\circ^2} \approx 1 - 1.2\left(\frac{D}{\Lambda}\right)^{2/3} \tag{6}$$

with σ being the SODAR σ_w, $\sigma_\circ$ the sonic or true unfiltered σ_w, and D the diameter of the crossection of the beam corresponding to the half power beam width. It should be noted that the linear dimension of the beam must be smaller than Λ. They applied this result to SODAR data, estimating Λ. Their comparison of corrected SODAR σ_w with reference σ_w was poorer than in the case of uncorrected SODAR σ_w. Their conclusion was that the difference between SODAR and sonic σ_w did not originate from volume filtering. We cannot apply this correction factor to the SODAR σ_w during the long term comparison. However, it will be shown in the second part of our experiment that this correction factor is not always valid.

4 Vertical velocity Spectra

4.1 Analysis of instantaneous data

4.1.1 Sonic autospectra

Two main facts concerning the time series and spectra of the sonic data can be summarized:

(i) The sonic data were sampled every 1.06 s. Although it is possible to compute a spectrum with such a sampling rate, one cannot calculate cross correlations with the SODAR data, because the SODAR sampling rate is different. It is necessary to transform the sonic data to obtain SODAR and sonic data at the same time (the transformed sampling rate was chosen to be 1 s).

(ii) The theory of spectral analysis makes the assumption that the power spectra or non–normalized spectral density is very low at and above the Nyquist frequency n_o. Aliasing folds power at frequencies higher than n_o back into the relevant spectrum. One practical solution to overcome this problem is to low-pass filter the data with half power at n_o. This restores the true power at n_o and reduces the effect of aliasing below this limit.

To take care of these two aspects, sonic data were filtered with an interpolation scheme using Cressman weight functions (Jones, 1972) to transform the 1.06 s sampling to a 1 s sampling. The low-pass filter has its half power at roughly 0.5 Hz. A detailed description is given in Appendix C.

The spectra were computed by Discret Fourier Transform (DFT) of the autocovariances with a Tukey-Hanning spectral window. The truncation point M follows from the rules described by Priestley (1981), and presented in Appendix A. The DFT routines have been described by Jenkins and Watts (1968).

4.1.2 SODAR autospectra

As described in section 2.1.2, the SODAR data in the instantaneous mode are not regulary distributed, and the missing data blocks are generally up to 15 s long. Figure 5 depicts the density function $f_1(t)$ of the SODAR sampling intervals during run No 5. This function indicates, for example, that in about 24% of all cases, the time between sequential sampling intervals is 2 to 3 s. The influence of small calibrations is seen in the decrease of $f_1(t)$ for an interval between sampling of 7 up to 9 s, whereas $f_1(t)$ is 2 times greater when the interval is 9 to 10 s. An example of SODAR and sonic time series during run No 5 is presented in Figure 6.

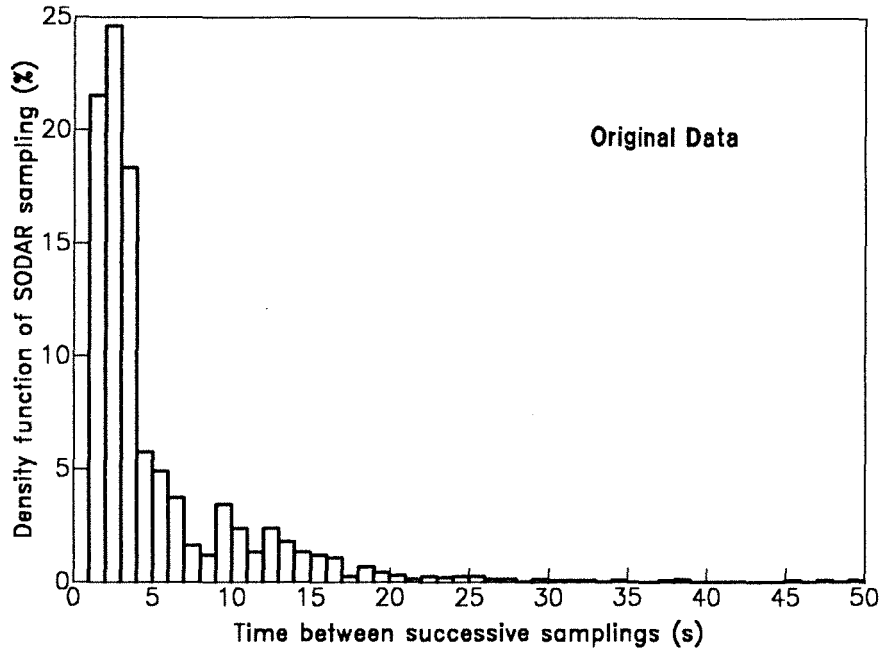

Figure 5: Density function of the SODAR sampling intervals, run No 5.

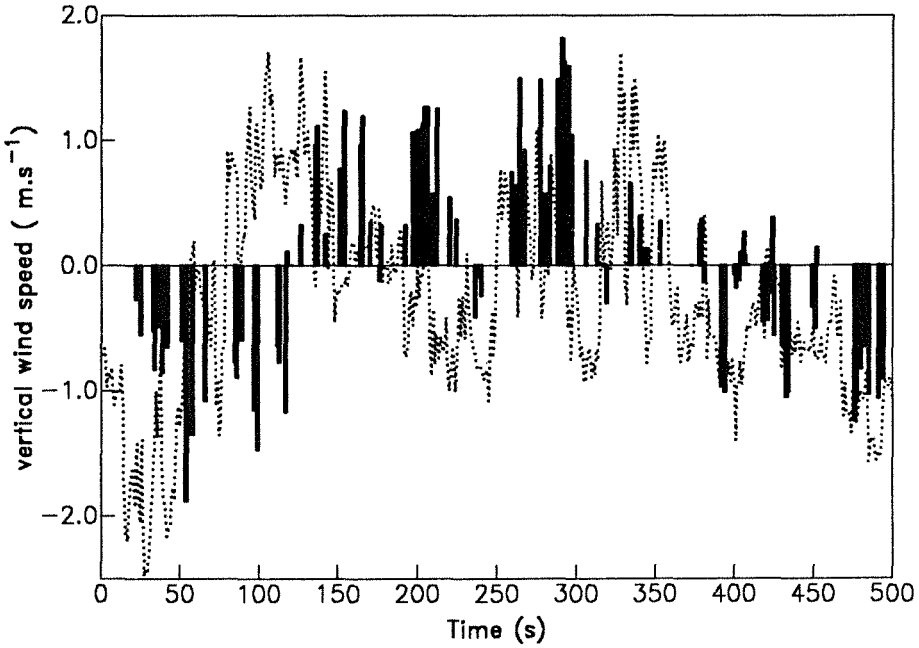

Figure 6: SODAR and sonic time series during run No 5. Sonic data are represented by the dotted line.

The theory of spectral analysis with randomly missing observations has been developped by Jones (1962), Parzen (1962), (1963), Scheinok (1965), Bloomfield (1970), Brillinger (1972), (1983), Dunsmuir and Robinson (1981) and others. The work of Parzen is the basis of these new theories. He has developed the concept of amplitude modulated stationary time series and has applied it to the case in which observations are missing in some periodic way. Bloomfield found conditions under which consistent estimates of the spectrum of the observed process can be made. Below, we summarize the main aspects of this concept and apply it to SODAR data transformation. For a more detailed description, Appendix B reviews the theory of amplitude modulation and its application to spectral analysis.

A time series with missing observations can be regarded as an amplitude modulated version of the original time series:

$$Z(t) = g(t)\,W(t)$$

where

(i) W(t) is the vertical wind speed under study, assumed to be defined at equally spaced points of time, with zero mean value.

(ii) g(t) is defined by

g(t) = 0 if W(t) is missing at time t.

g(t) = 1 if W(t) is observed at time t.

(iii) Z(t) represent the observed sequence of W(t), with 0 inserted in the time series whenever the value of W(t) is missing.

We are thus able to calculate the spectrum of the time series Z(t). But this spectrum, denoted $S_z(\omega)$, is not a good estimate of the real spectrum $S_w(\omega)$. One can show that

$$S_z(\omega) = C_g^2 \left[S_w(\omega) + \int_{-\pi}^{\pi} A(\omega - \theta) S_w(\theta)\, d\theta \right] \qquad (7)$$

where C_g and the function $A(\omega)$ are due to the properties of the sampling scheme $g(t)$. If all data were observed, we would have C_g=1 and $A(\omega) = 0$. This fundamental relation (7) was set down by Bloomfield for discrete real valued time series, and by Brillinger (1972) and Marsy(1978) for continuous real valued time series. Eq. (7) makes it clear that the spectrum of the observed time series reflects the properties of the true spectrum $S_w(\omega)$ and the properties of the sampling scheme. The conclusion of this discussion is that the percentage of missing data should be low, and the function $A(\omega)$ should correspond as closely as possible to white noise.

Table 4 indicates the percentage of observed data for all time periods when the SODAR was running in the instantaneous mode. Because of the lack of data, the confidence on the velocity spectra would be very poor. We are therefore obliged to use data transformation to increase the percentage of "available" data and to reduce the "spectrum" of the sampling scheme $A(\omega)$ to white noise.

One method to transform the function $A(\omega)$ would be to omit data in a random way, but in this case the percentage of missing data is already too high. A second method would be to average data in non overlapping blocks. But in a period of two hours, using an averaging interval of 10 s, only 720 blocks are available for spectral analysis. It is not possible to obtain great confidence, in the statistical sense, in the spectra with so few data.

Table 4: Percentage of availability of the observed and transformed data.

Run No	Date	Time (CET)	% of observed data	Mov. av. length (s)	% of transf. data
1	01/08/1990	13h09-15h12	11.1	7	46.3
2	10/08/1990	10h41-12h36	16.2	5	50.7
3	15/08/1990	09h50-11h40	13.1	5	44.1
4	16/08/1990	17h20-18h40	16.9	3	40.1
5	04/09/1990	14h19-16h30	21.7	5	65.1
6	05/09/1990	10h58-13h15	20.6	5	61.3
7	11/09/1990	08h22-10h39	25.7	5	70.4

The third method is to transform the data using a moving average of overlapping blocks. The moving average procedure (Cressman weighting) consists of estimating the value at each data point with an average of the data separated by 1 to 3 s from the data point in question. Below 0.05 Hz, this procedure has a similar effect to a symetric low-pass filter that is, it does not introduce shift. The percentage of observations is greatly increased in all the cases, as shown in Table 4, which illustrates the effect of the moving average transformation for averaging length of 3, 5, and 7 s.

4.2 Spectra of the vertical velocity component

The seven time series were between 1 and 2 hours long, were measured during the day, and cover a wide range of stability situations. Table 5 lists the mean wind speed and direction measured by cup-anemometers and wind-vanes, the standard deviation of direction σ_θ measured by propvanes, the temperature, and the gradient Richardson number all at 100 m AGL.

Table 5: Significant mean meteorological parameters measured on the tower at 100 m AGL during the seven runs.

Run No	Temp. $°C$	Speed U (ms^{-1})	Direction θ (degrees)	σ_θ (degrees)	Richardson number
1	29.3	5.7	71	15.0	-0.54
2	24.1	4.6	245	13.9	-2.10
3	21.2	6.4	227	10.1	-1.57
4	16.5	7.9	252	7.0	0.17
5	17.7	6.5	229	6.2	0.18
6	14.7	3.9	242	13.7	-1.80
7	11.7	1.6	321	16.0	-0.10

Unfortunately, due to instrument failure, all values of σ_θ in August had to be measured by windvane. These values (runs No 1 to 4) have been corrected by a factor 1/1.3, because in previous studies it was found that the windvane overestimates σ_θ by a factor of about 1.3. To calculate the gradient Richardson numbers (Arya, 1988), wind and temperature gradients were found by differentiating second order polynomials fitted to average speeds and temperatures measured near the level in question (L.Mahrt *et al.* (1979), Kaimal *et al.* (1976)). In most cases five levels were used for each computation, namely the level itself, the two below and the two above. The polynomials were in $\ln(z)$ for the wind speed and in z for the temperature (z is indicating the height above ground level).

In the discussion to follow, we will use common meteorological notations. We use frequencies, not wave numbers, and the conversion between them is made through the use of the Taylor hypothesis. We introduce the following notation:

n	frequency
$f = nU/z$	non dimensional frequency
k	wavenumber
n_m	frequency of the logarithmic spectral peak
$\lambda = U/n$	wavelength
$\lambda_m = U/n_m$	outer turbulent scale wavelength corresponding to the peak of the logarithmic spectrum
Λ	integral scale of turbulence

It is traditional in atmospheric work to plot frequency spectra $S_w(n)$ and $n\,S_w(n)$, not against the frequency n, but against the non dimensional frequency f. However, the purpose of this study is to discuss the physical limitations of the systems, therefore we will use $\log(n)$ as abscissa and $\log(n.S_w(n))$ as ordinate to simplify the study. The spectral forms will be referred to as logarithmic spectra.

Although the sampling rate of the transformed SODAR data was about 1 Hz, the SODAR spectra have been removed for frequencies above 0.15 Hz. Above this frequency, the confidence level in the statistical sense for the spectra is very poor, as shown in Appendix B (see the 80% confidence interval of the SODAR logarithmic spectrum for each run).

The spectra of the vertical wind speed derived from SODAR measurements should be the same as those derived from the sonic anemometer. Due to the configuration of the system, the SODAR sampling volume is large, which causes attenuation of the SODAR spectra for high frequencies. Other authors have discussed this matter for RADAR (Srivastava and Atlas (1974)) and SODAR (Gaynor (1977), Kaimal *et al.* (1984)). Assuming a Gaussian

illumination function, which appears appropriate for SODARs, Srivastana and Atlas suggested that the three dimensional filter function corresponding to the pulse volume is

$$\phi_r(k) = \left(\frac{\sin k_1 L/2}{k_1 L/2}\right)^2 exp(-\sigma^2 k_2^2)\, exp(-\sigma^2 k_3^2) \tag{8}$$

where

- k_1, k_2, and k_3 are the three orthogonal components of the wavenumber, k_1 is along the vertical beam axis.
- $L = h/2$, with h the pulse length along the beam axis.
- $\sigma = 0.3D$, with D, the horizontal dimension of the beam corresponding to the half power beam width.

Wavelengths which are small compared to the SODAR sampling volume are filtered whereas wavelengths for which $\lambda_1 > 4L$ and both λ_2 and $\lambda_3 > 4D$ are unaffected. Srivastava and Atlas (1974) have illustrated this result with numerical calculations, and have also shown that one dimensional spectra are attenuated, even at scales which are large compared to the beam dimension. This is because the one dimensional spectrum has a contribution from small wavelengths orthogonal to the beam direction, which are attenuated under these conditions. According to their interpretation, the filtering causes a lessening of the power in the inertial subrange above the frequency n_f, the extend of which depends on the variable relationship between the sampling volume and the outer turbulence scale wavelength.

In our case, D and L are about 25 m and 20 m respectively at 100 m AGL. The cutoff frequency n_f should be roughly

$$n_f = \left(\frac{U}{4D}\right) . \tag{9}$$

4.2.1 Comparison during unstable conditions

The runs recorded during unstable conditions are No 1, 2, 3, 6 and 7.

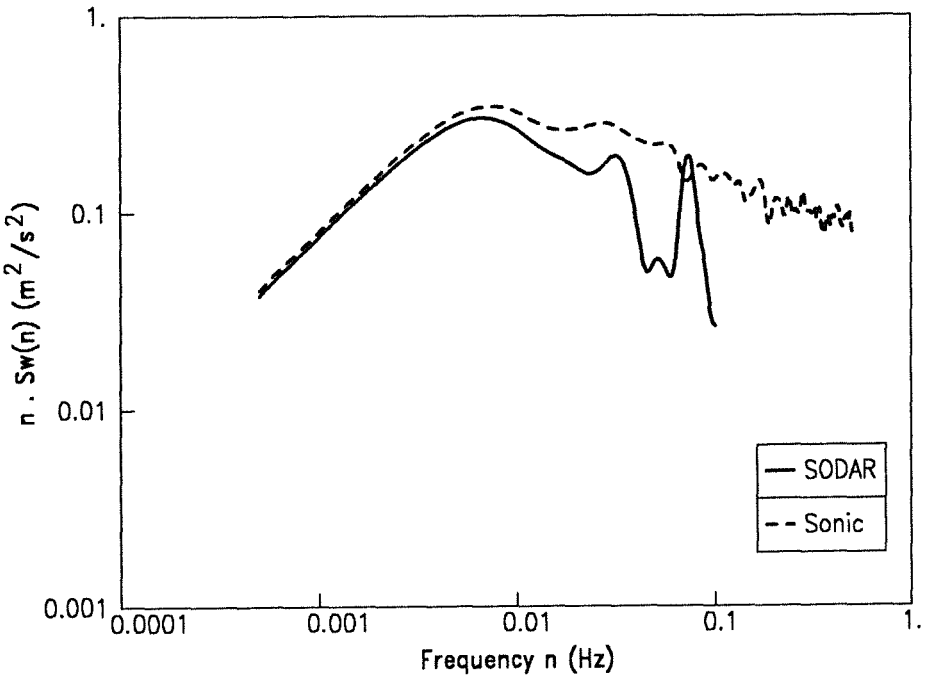

Figure 7: Vertical velocity spectra, run No 1 (01/08/90).

Although the sonic anemometer was in the wind shadow from time to time during run No 1 (Figure 7), this does not seem to have had a great effect on the estimation of the logarithmic spectral peak. It may disturb the small scale turbulence, but the spectral density for $n \leq 0.03\ Hz$ appears to remain unaffected. Because the percentage of available SODAR data was low, it was necessary to average data over 7 s blocks. The sharp minimum in the range 0.03 Hz to 0.07 Hz is due to the SODAR sampling scheme.

Concerning run No 2 (see Figure 8), the power of the SODAR spectrum at $\approx 0.025\ Hz$ is underestimated because of missing data. At frequencies above 0.1 Hz, the logarithmic spectrum derived from SODAR data decreases because the low-pass filter transfer function has its -3dB point at roughly this frequency. The sharp minimum at approximately 0.08 Hz is due to the sampling process. This coincides with the presence of a minimum in the density function of the sampling process due to the small calibrations (see Figure 5 and Appendix C, Figure 36).

The results from run No 3 (Figure 9) show that the spectra have the same shape, but the SODAR underestimates the power at all frequencies. However, the logarithmic spectral peaks are well defined and are nearly the same.

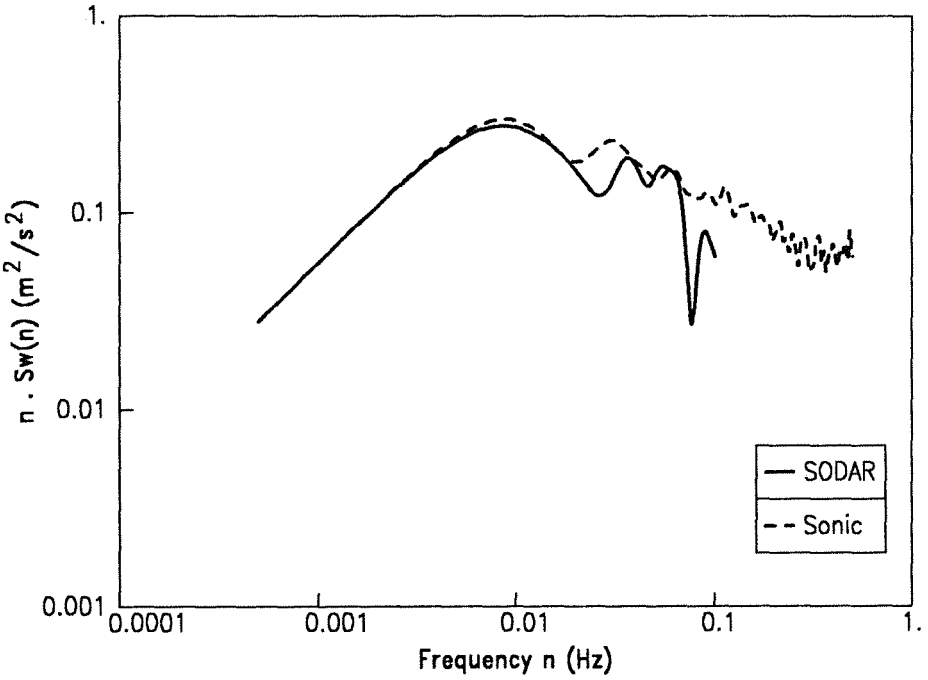

Figure 8: Vertical velocity spectra, run No 2 (10/08/90).

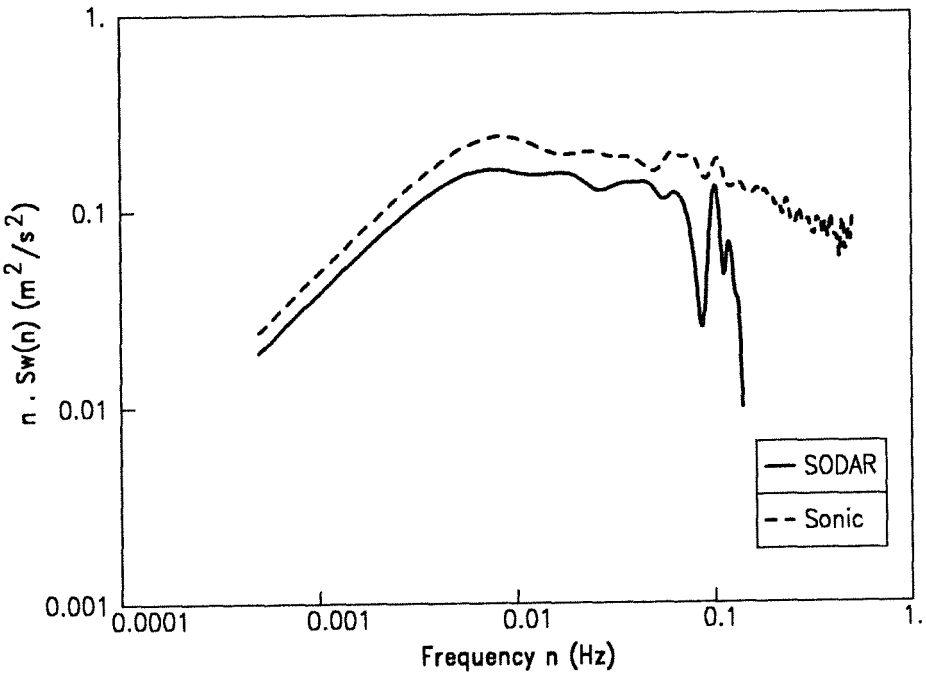

Figure 9: Vertical velocity spectra, run No 3 (15/08/90).

The results from run No 6 (Figure 10) show that, in typical convective conditions, the SODAR and sonic spectra are identical for frequencies up to 0.02 Hz. For frequencies between 0.02 Hz and 0.07 Hz, the spectra have the same shape, but the SODAR underestimates the power.

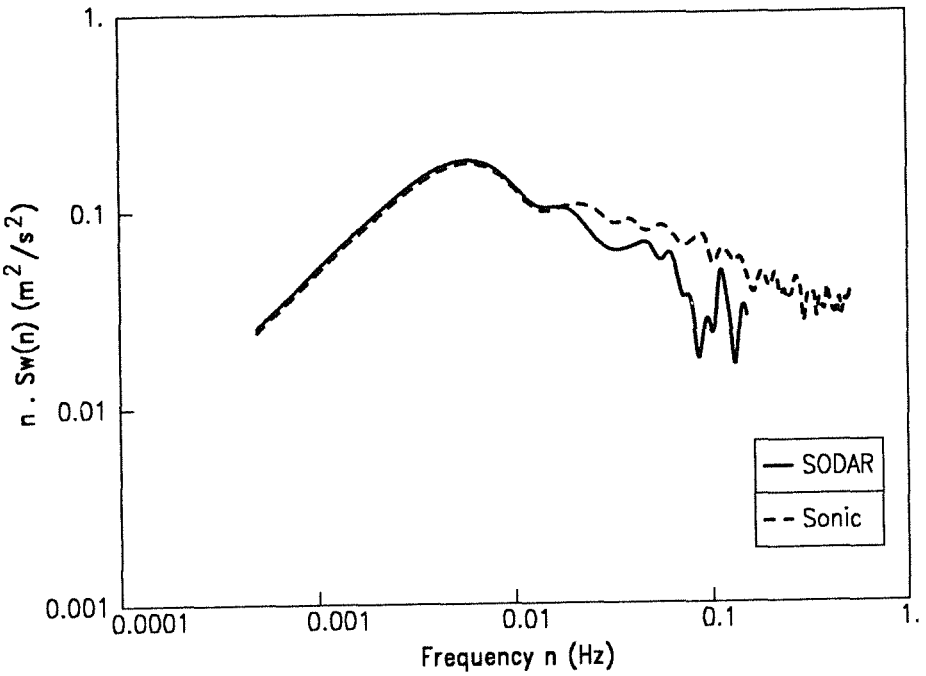

Figure 10: Vertical velocity spectra, run No 6 (05/09/90).

Run No 7 (Figure 11) took place early in the morning. Before 09h00 CET a strong wind shear was present at roughly 100 m with a very low wind speed ($\approx 1\ ms^{-1}$), which disappeared between 09h30 and 10h00 CET. Figure 12 depicts the variations of wind speed at 100 m AGL, the wind direction at 40 m AGL and 160 m AGL, and the temperature at 100 m AGL. The logarithmic spectrum derived from SODAR data is underestimated by a factor that is approximately constant. To investigate this problem, we have computed a sonic spectrum with the same sampling scheme as the SODAR data for runs No 6 and No 7 (Figures 13 and 14).

Figure 13 shows a fair agreement between the SODAR and sonic spectra under the homogenous turbulence conditions which were present during run No 6. Figure 14 illustrates the situation in wind shear conditions (run No 7). The agreement between the sonic and SODAR spectra is still poor, and the underestimation of the power is the same as in Figure 11.

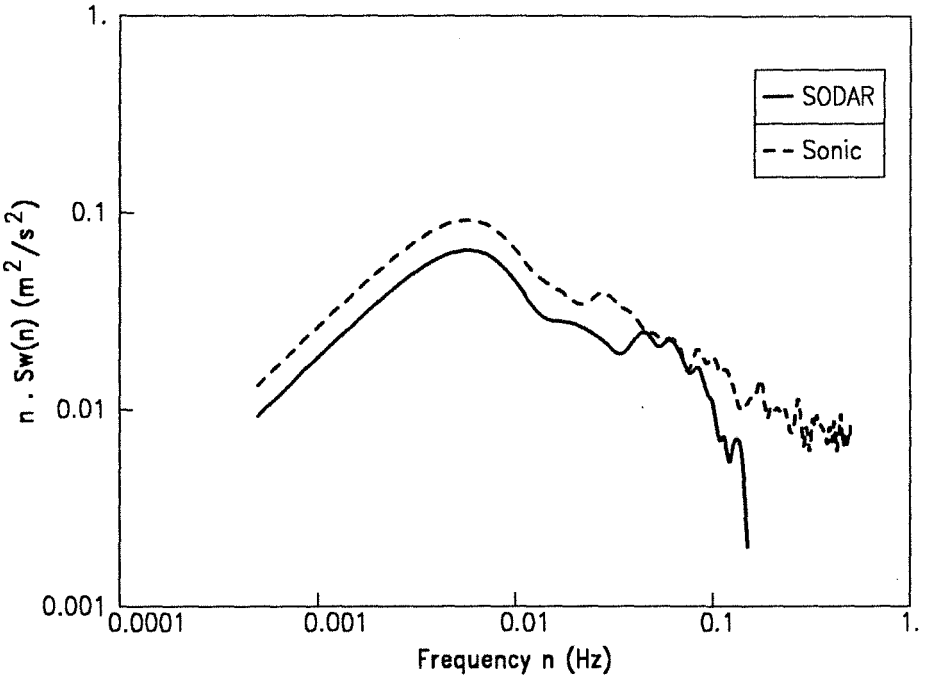

Figure 11: Vertical velocity spectra, run No 7 (11/09/90).

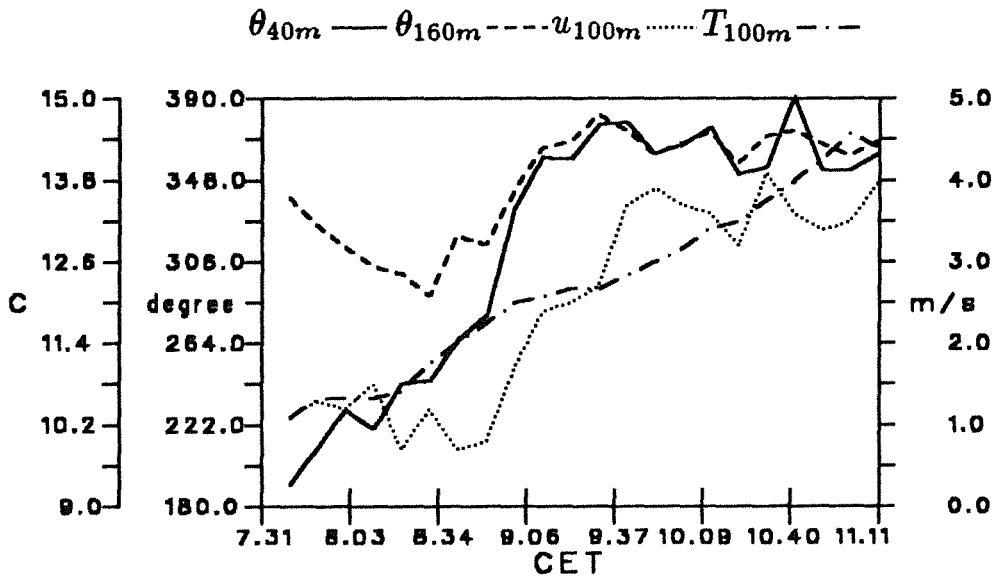

Figure 12: Wind direction (θ), speed (u), and temperature (T) between 40 m and 160 m AGL, 11/09/90.

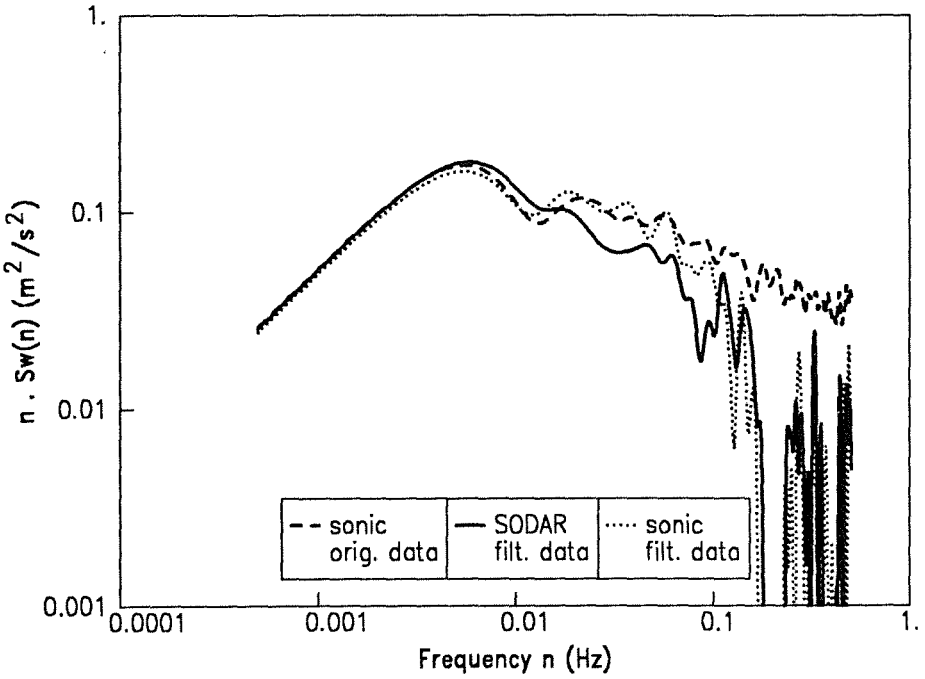

Figure 13: Vertical velocity spectra, run No 6 (05/09/90).

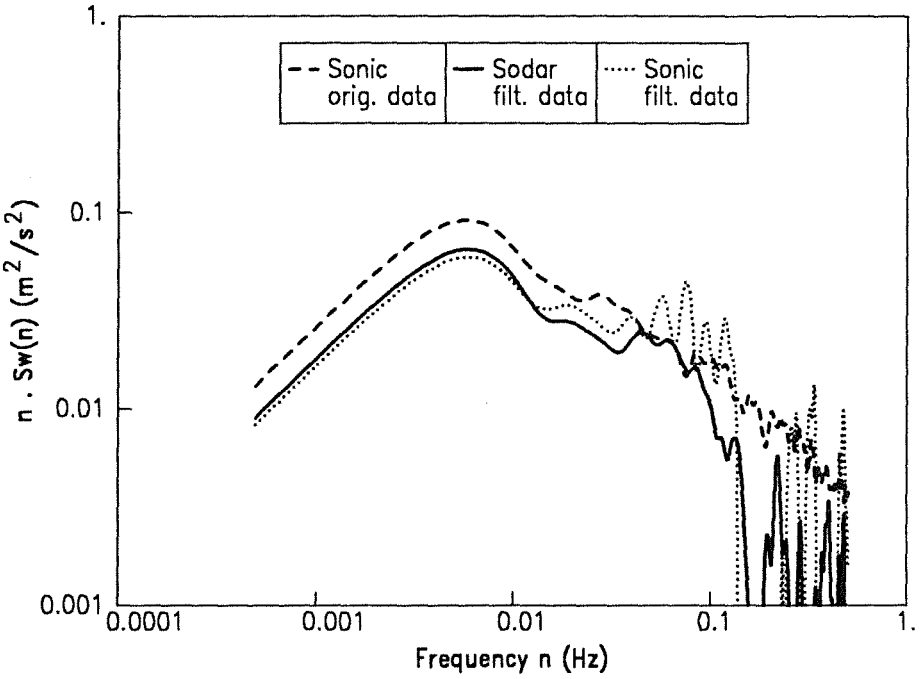

Figure 14: Vertical velocity spectra, run No 7 (11/09/90).

Therefore, this underestimation is not due to the sampling scheme but presumably due to the fact that the two systems did not detect the same turbulence fluctuations.

This study reveals three different kinds of spectra:

(i) The runs No 1, 2, and 6 show similar trends, with high power levels. The inertial subrange with $-2/3$ slope is well defined. In all cases, the logarithmic spectral peak derived from SODAR is very close to that derived from the sonic spectra. Above 0.03 Hz, the influence of missing data and spatial averaging reduces the accuracy of the SODAR spectra.

(ii) The run No 3 reveals that in some cases the SODAR underestimates the spectrum.

(iii) The run No 7 is uncommon, because the atmospheric situation is changing during the experiment. Even if the SODAR underestimates the spectrum, the SODAR and sonic logaritmic peaks are close.

4.2.2 Comparison during stable conditions

The prevailing atmospheric conditions during run No 4 (Figure 15) and run No 5 (Figure 16) were weakly stable. The high wind speed at 100 m AGL ($\approx$ 8 ms^{-1} during run No 4 and $\approx$ 6 ms^{-1} during run No 5) has the expected effect on the spectra: The logarithmic spectra are shifted to higher frequencies. Note that the light rain (4 mm/hour) during the whole run No. 4 did not perturb the SODAR. The sonic spectra of both runs have nearly the same shape, however the spectra derived from SODAR data are underestimated. This is not surprising, considering the following facts:

(i) During stable conditions, the logarithmic spectral peaks are shifted to higher frequencies and have lower power. This is a disavantage for the SODAR which cannot detect small scale turbulence eddies.

(ii) The correction for missing data does not completely restore the spectrum because the peaks of the SODAR spectra are situated on the high part of the spectral bandwidth, and also the SODAR spectra have a poor confidence interval (see Appendix B).

(iii) The sampling volume filtering reduces the power of the SODAR spectra in the spectral window above 0.08 Hz (run No 4) and 0.06 Hz (run No 5), following Eq. (9).

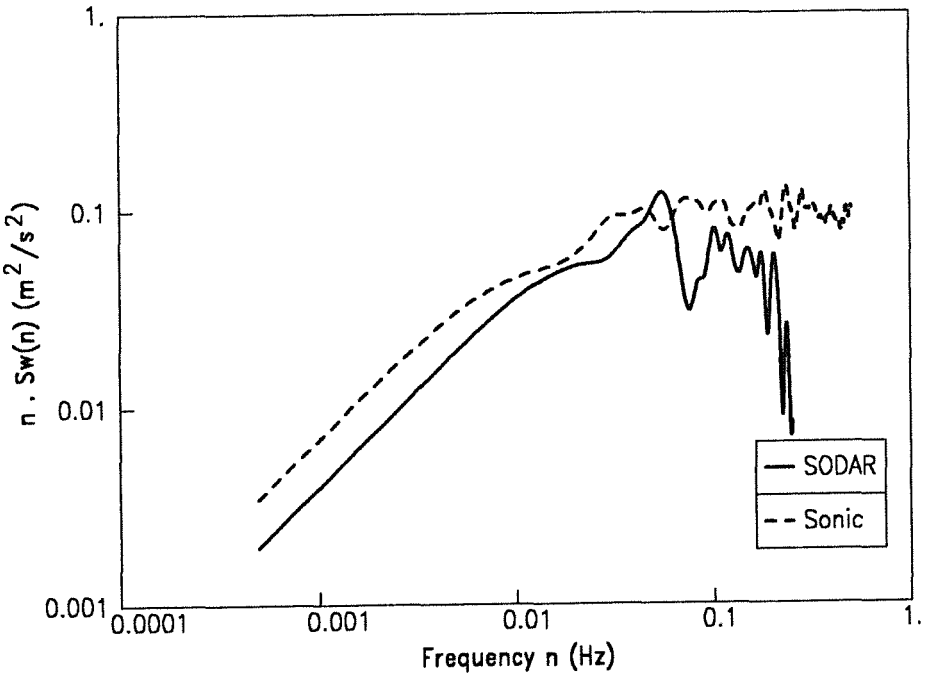

Figure 15: Vertical velocity spectra, run No 4 (16/08/90).

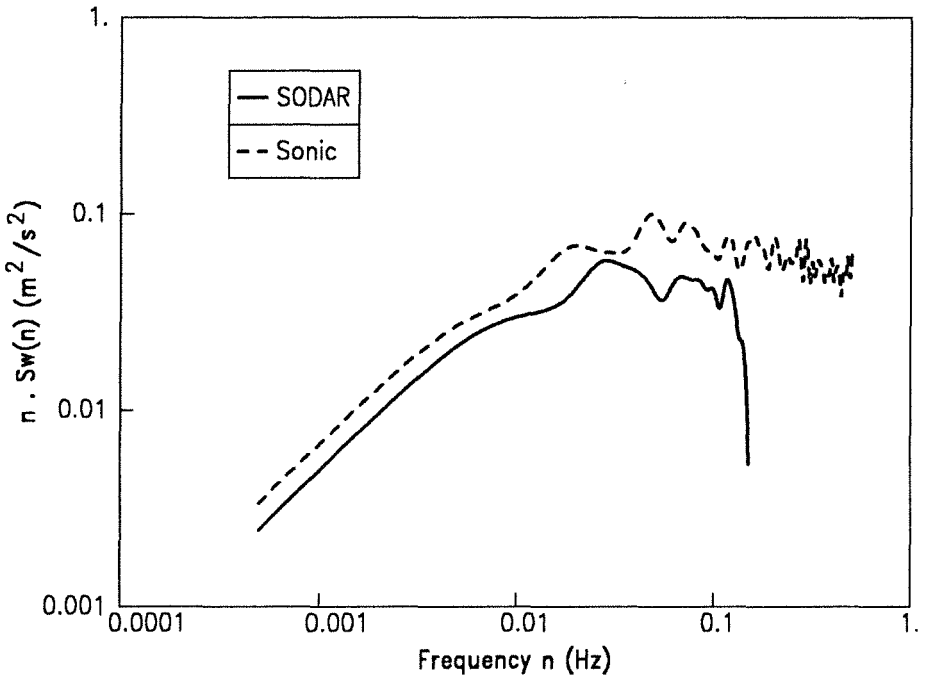

Figure 16: Vertical velocity spectra, run No 5 (04/09/90).

According to Figures 15 and 16, it is difficult to estimate the logarithmic spectral peak with good accuracy. We have computed a sonic spectrum with the same sampling scheme as that of the SODAR data for the run No 5. Figure 17 shows that the power of the SODAR spectrum is lower than that of the sonic spectrum. The SODAR spectrum departs markedly from the sonic spectrum at high frequencies, presumably due to the filtering of power by the sampling volume.

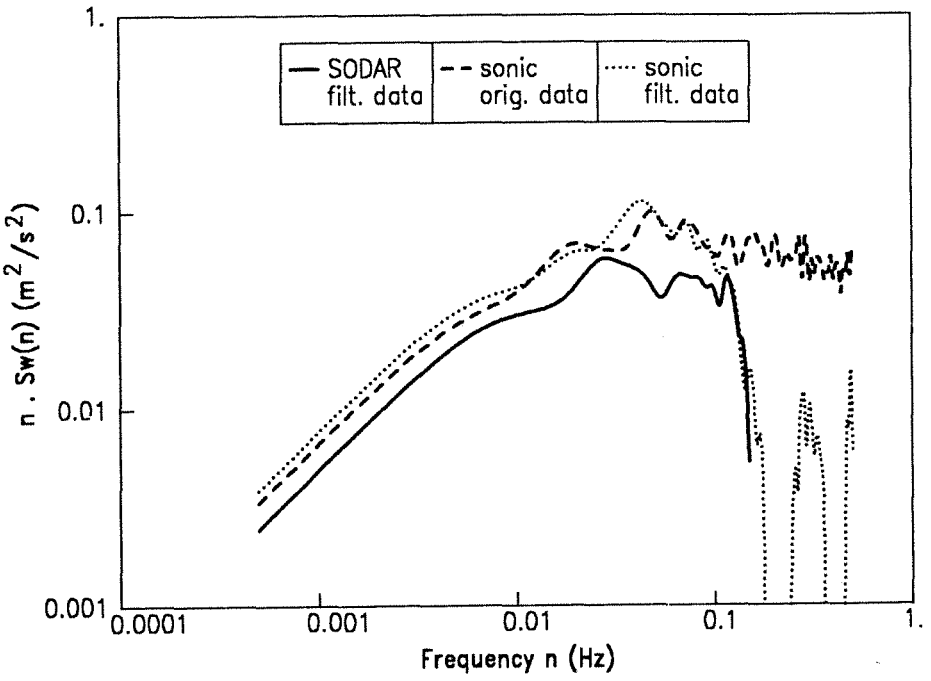

Figure 17: Vertical velocity spectra from SODAR and sonic data with the same sampling scheme. Run No 5 (04/09/90).

4.2.3 Characteristic scales of turbulence

Several methods for estimating the characteristic scales of the energy-containing eddies can be found in the literature. Two that are commonly used refer to the wavelength λ_m corresponding to the peak of the logarithmic power spectrum and to the integral scale Λ:

$$\Lambda = U\tau = U \int_0^\infty \rho(t)\, dt \tag{10}$$

where $\rho(t)$ is the autocorrelation coefficient and τ is the integral time scale.

The peak wavelength λ_m is important for studies of turbulent transport in the boundary layer and we have therefore examined it. Figure 18 shows the SODAR and sonic λ_m for stable and unstable conditions. As illustrated in this figure, the SODAR is able to measure the outer turbulent scale wavelength with good accuracy in all atmospheric situations. The corresponding relative precision is about 7 %.

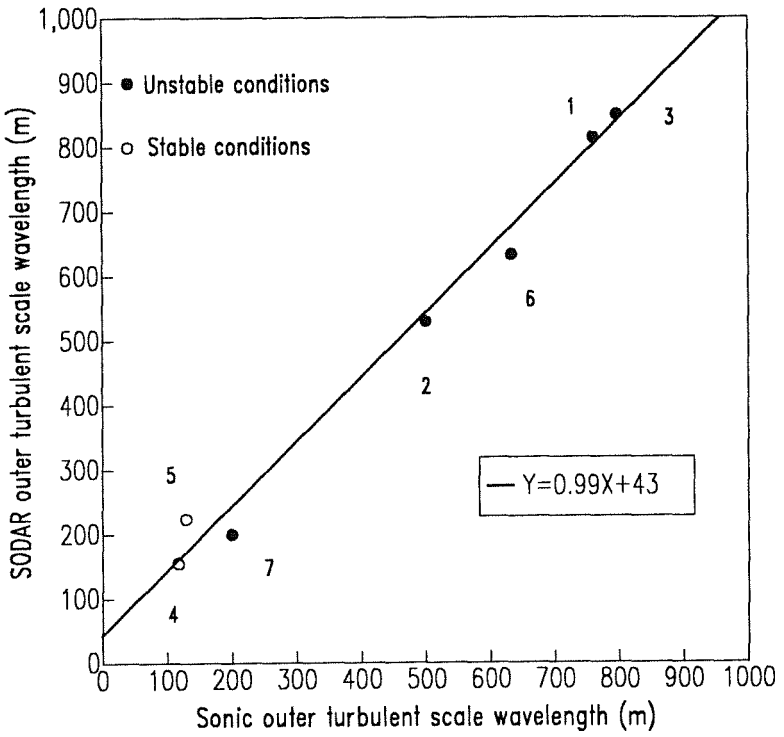

Figure 18: Outer turbulent scale wavelength λ_m estimated from SODAR and sonic data. The figures refer to the run No.

Λ can be determined from the spectrum by extrapolating the low-frequency roll-off to zero frequency. Theoretically one needs a record of infinite length in order to estimate τ. However, due to limitations imposed by a finite observation time, one makes a simple extrapolation of the autocorrelation or the spectrum. As indicated by Kaimal (1972), the measured Λ then represents the actual length scale at moderate to high frequencies. Fortunately, a large gap usually exists between spectral regions representing turbulent energy and those representing the energy of long-term oscillations. Kaimal has proposed under these conditions to estimate Λ with the following relation :

$$\Lambda = \frac{1}{4} U \frac{S_w(0)}{\sigma_w^2} \tag{11}$$

Table 6 indicates the integral scales of turbulence for the 7 runs. Figure 19 illustrates the two atmospheric situations. The RMSE of SODAR Λ is about 18 m, which leads to a relative precision of about 22%. The SODAR is not as accurate when measuring the integral scale as when measuring the wavelength corresponding to the logarithmic spectral peak. This is due to the SODAR σ_w^2 error which has a great influence on the integral scale estimation.

We have used the values of the integral scale to predict the correction

Table 6: Sodar and sonic turbulence parameters.

Run No	SODAR $S_w(0)$ $(m^2 s^{-1})$	Sonic $S_w(0)$ $(m^2 s^{-1})$	SODAR σ_w^2 $(m^2 s^{-2})$	Sonic σ_w^2 $(m^2 s^{-2})$	SODAR Λ (m)	Sonic Λ (m)
1	76	81	0.87	1.34	123	86
2	56	56	0.82	1.03	76	61
3	38	48	0.61	0.99	99	78
4	4	7	0.25	0.40	32	34
5	5	7	0.17	0.31	45	34
6	51	49	0.55	0.60	77	101
7	18	26	0.19	0.27	38	39

coefficient for σ_w as indicated in Eq. (6) and as described by Kristensen and Gaynor (1986). In unstable conditions (runs No 1, 2, 3, and 6), the observed ratio $\sigma^2_{SODAR}/\sigma^2_{sonic}$ is 0.6-0.9, whereas the predicted ratio is 0.35–0.5. However, during run No 7, which is slightly unstable, the integral scale of turbulence is small and the predicted ratio 0.1 greatly underestimates the observed ratio 0.7.

Under the stable atmospheric conditions (runs No 4 and 5), the observed ratio of 0.55–0.65 greatly exceeds the predicted ratio of 0.1. The correction factor of Kristensen and Gaynor is no longer valid when the integral scale is of the same order of magnitude as the sampling volume, which is the case for the two stable runs.

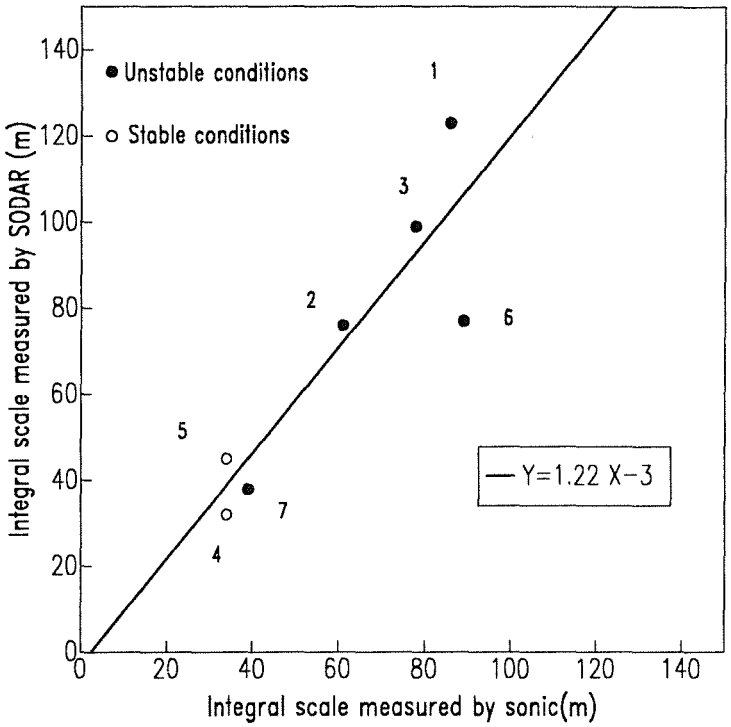

Figure 19: Integral scale of turbulence Λ estimated from SODAR and sonic data. The figures refer to the run No.

4.3 Conclusions

The conclusions to emerge from this study can be summarized as below:

(i) Although the SODAR is missing data and the SODAR antenna configuration filters the high frequency turbulence, the vertical wind speed spectra derived from SODAR are in general comparable to the spectra derived from sonic data. In windy conditions, however, the inertial subrange slope lacks detail because of the low sampling rate.

(ii) In all unstable atmospheric conditions, the logarithmic spectral peaks measured by SODAR and sonic are very similar. The characteristic

outer turbulent scale wavelength λ_m deduced from n_m, and the integral scale of turbulence Λ obtained from SODAR and sonic are, in all atmospheric conditions, also very similar.

(iii) The SODAR data transformation and the modulated amplitude theory are satisfactory. The SODAR logarithmic spectra have 80% confidence intervals which include nearly all frequencies of the sonic spectra. The correction is, however, better in unstable conditions and low to medium wind speeds, because the logarithmic spectral peak is then not contaminated by the influence of the periodic small calibrations.

(iv) One can interpret the underestimation of the spectrum by SODAR in stable conditions as being the result of the difference between physical phenomena in stable and unstable conditions: In stable situations, the eddies are small, corresponding to mechanical or frictional forces, while in unstable atmospheric conditions, the eddies resulting from heat convection are greater and are more easily detected by the SODAR.

5 Crosscorrelations and crosspectra

5.1 Theoretical Background

The crosscovariance is of interest because of the quantitative information on the temporal correlation of instantaneous vertical wind speed measured by SODAR and sonic.

When dealing with missing data, it is possible to use the same method to determine crosscovariance, crosscorrelation, and crosspectrum as for autocovariance, autocorrelation, and autospectrum (presented in Section 4. In this case, the two time series involved can be regarded as amplitude modulated versions of the original time series. With the help of the following relation, we have computed crosscovariance, crosscorrelation, and crosspectrum following (Brillinger, 1972):

$$R_{z\acute{z}}(r) = R_{g\acute{g}}(r) R_{w\acute{w}}(r) \tag{12}$$

with $R_{z\acute{z}}(r)$ being the crosscovariance of observed time series $Z(t)$ and $\acute{Z}(t)$, $R_{w\acute{w}}(r)$ the crosscovariance of original time series $W(t)$ and $\acute{W}(t)$, and $R_{g\acute{g}}(r)$ a function depending on the sampling schemes $g(t)$ and $\acute{g}(t)$. The computation of crosscorrelations and crosspectra is done following Jenkins and Watts (1968), and Priestley (1981).

5.2 Results and conclusion

There are a number of reasons why the two systems may show different readings of w at the same time. The distance between the two sensors does not permit measurements within the same volumes and the same eddies, except for the particular case in which the wind direction is parallel to the direction of the SODAR-tower. Unfortunately, this never occurred during the seven runs.

A localy isotropic homogeneous turbulence and a "frozen atmosphere" (Taylor hypothesis) is assumed. The correlation between vertical wind speed at two points A and B is given by (Hinze, 1959):

$$\overline{(w')_A (w')_B} = \sigma_w^2 \left[\frac{f(r) - l(r)}{r^2} \xi_w^2 + l(r) \right] \tag{13}$$

where r is the distance between A and B, ξ_w is the distance between A and B along the vertical axis, $f(r)$ is the vertical correlation along the vertical axis, and $l(r)$ is the lateral correlation (isotropic within horizontal plane). In our case, with A and B at the same altitude, ξ_w is equal to zero and the correlation is equal to $l(r)$. As a first approximation, one may consider that the autocorrelation of wind speed follows an exponential law (Hinze, 1959). Then, the correlation $\rho(r)$ is :

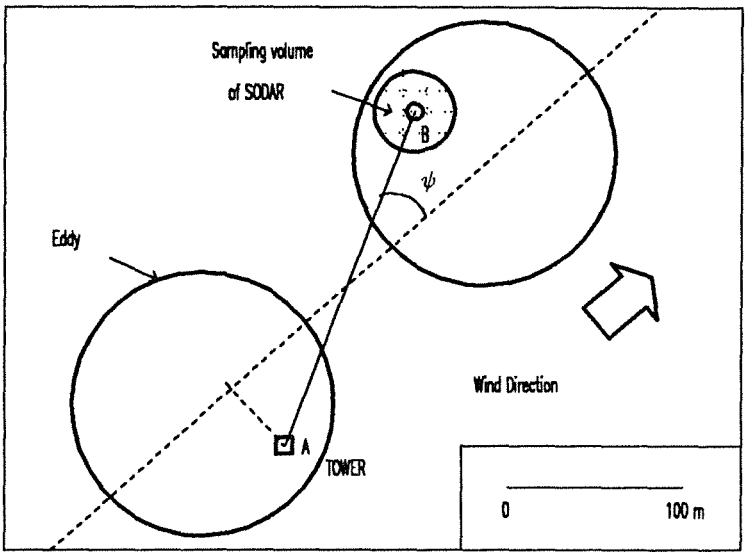

Figure 20: Example of SODAR and sonic positions in the wind field. Run No 3 (15/08/90).

$$\rho(r) = l(r) = \frac{\overline{(w')_A (w')_B}}{\sigma_w^2} \approx e^{-\frac{r}{\Lambda}} \tag{14}$$

Appling this theory by way of example to run No 3 with $r \approx 200\ m$ and $\Lambda \approx 100\ m$ gives $\rho(r) \approx 0.13$.

Some authors have investigated the relation among wind speed U, wind direction, and the time lag τ_m at which the lateral correlation becomes maximum (see for example Shiotani and Iwatani, 1976). Here, the time that turbulent eddies travel from point A to point B should be proportional to $r \cos\psi / U$ (ψ denotes the angle between the wind direction and the SODAR-sonic line in Figure 20). The correlation between SODAR and sonic should become maximal when the time lag is equal to $r \cos\psi / U$. For run No 3, $U/\cos\psi \approx 7\ ms^{-1}$ and the time lag $r \cos\psi / U$ is about 29 s.

Table 7 shows the maximum and minimum cross correlations, the time lag τ_m, and time lag $r \cos\psi / U$ for all runs. The very poor correlations seem to be of the same order as the theorical values from Eq. (14). Furthermore,

if SODAR and sonic data were correlated, the time lag in Table 7 would have been proportional to $r\cos\psi/U$, but this was not the case (it has been found by Shiotani and Iwatani that there is a proportionality coefficient of about 0.8 between τ_m and $r\cos\psi/U$). It is clear that in none of the runs is it possible to make a direct comparison of SODAR and sonic instantaneous vertical wind speed.

Table 7: List of maximum and minimum crosscorrelations between SODAR and sonic, time lag τ_m for maximal correlation, and time lag $r\cos\psi/U$.

Run No	Maximum cross corr.	Minimum cross corr.	Time lag τ_m (s)	$r\cos\psi/U$ (s)
1	0.008	-0.210	200	-25
2	0.102	-0.119	-186	34
3	0.184	-0.117	66	29
4	0.103	-0.131	-12	18
5	0.111	-0.093	35	28
6	0.130	-0.110	-76	41
7	0.112	-0.030	-224	53

6 Conclusions

The long term intercomparison showed that, in general, the σ_w data of the SODAR compare well with the sonic anemometer data. The agreement between both sets of data is much better during the nighttime measurements; this means that the SODAR σ_w values are more accurate during stable than during unstable atmospheric conditions. There is, however, an underestimation of σ_w measured by the SODAR especially at higher wind speeds.

The spectral analysis of the vertical wind speed showed that during different atmospheric conditions the SODAR can truly observe large to small scale turbulence eddies. In special situations, even fluctuations down to the inertial subrange are observable. The peak of the logarithmic spectrum is accurately determined by the SODAR in all cases, although in some runs the power spectra derived from SODAR data are too low. The reasons for this are not clear. More tests are needed to understand the physical meaning of this effect. In addition, the outer turbulent scale wavelength corresponding to the peak of the logarithmic spectrum and the integral length scale of turbulence are also accurately determined by the SODAR. Both parameters are associated with the vertical transport of pollutants.

The mathematical approach of the spectral analysis which has been presented provides some topics for future study. Turbulence fluxes as $u'w'$ or $w'T'$ may be derived from SODARs or a combination SODAR-RASS (the RASS is a Radio Acoustic Sounding System which permits measurements of temperature profiles within the Planetary Boundary Layer). Further comparisons need to be performed in order to quantify the ability of the SODAR and RASS to measure these cospectra and fluxes to be used as an input to atmospheric models.

Appendices

A Comments on spectral analysis

The purpose of this Appendix is not to give a complete description of the notion of spectral analysis. Many authors (Jenkins and Watts,1968, and more recently Priestley,1981) have published complete studies of this subject. We present a short review of the main assumptions and results of spectral analysis theory. Some of the notations and results are used to explain the theory of amplitude modulation functions in Appendix B.

A.1 Spectral analysis theory

A time series is very often a random or non deterministic function of the time. A characteristic of these random functions is that they are not predictable. For example, if we compare visually the time series of vertical wind speed given by SODAR and sonic anemometer, they do not ressemble each other. But their averaged or statistical properties such as mean value or standard deviation are in good agreement (see Section 3.2).

We define a random process as the collection of all possible records of a random variable $X(t)$ and we note it $\{X(t)\}$. We use different symbols to refer to the observation $x(t)$ or x_t (discret sample) from the particular sample we have selected as opposed to the random variables $X(t)$ or X_t (discret sample) which denote general values of the observation at time t. For each value of t, there exists a whole range of possible values of $X(t)$. Thus, an observed record of a random process is merely one record out of a whole collection of possible records which we might have observed. The collection of all possible records is called the "*ensemble*", and each particular record is called a "*realization*" of the process. The sample space ("*ensemble*") associated with this process is doubly infinite, extending from $-\infty$ to $+\infty$ at each point of time and time extending from $-\infty$ to $+\infty$.

For each t, $X(t)$ is a random variable and thus has a range of possible values, some of which may be more likely to occur than others. Acoordingly, for each t, $X(t)$ will have some probability distribution. In most cases, its properties will be described by its probability density function $f_t(x)$, defined for all x at time t. We can then define the first and second moment of the random variable $X(t)$ (mean value $\mu(t)$ and variance $\sigma^2(t)$):

$$\mu(t) = E[X(t)] = \int_{-\infty}^{\infty} x f_t(x) dx \tag{15}$$

$$\sigma^2(t) = E[X(t)^2] = \int_{-\infty}^{\infty} x^2 f_t(x) dx\,, \tag{16}$$

and also the autocovariance function and all the higher moments. $E[X(t)]$ is the expected value of $X(t)$. $E[X(t)]$ is computed as a weighted average of

all possible values of $X(t)$, each value being weighted by the corresponding probability $f_t(x)$. Note that the moments of the probability law may vary with time. To describe a general theory of stochastic processes, it is necessary to make two assumptions to simplify the problem:

(i) The time series can be described with the lowest moments of its probability law: mean value, variance, autocovariance, and the Fourier transform of the autocovariance, which is named the power spectrum. This assumption is true in the particular case of normal probability law (Gaussian distribution).

(ii) The probability law during the time of measurement remains the same.

These assumptions can be applied to time series of atmospheric turbulence parameters that are approximately stationary during short time periods, like in our experiment. It has a lot of applications in meteorology such as spectral analysis of fluxes of various properties, and analysis of the relationship between two time series like wind speed and temperature.

Considering a stationary random process $\{X(t)\}$, the mean value μ, autocovariance $R(s)$ and autocorrelation $\rho(s)$ are independent of time t:

$$\mu = E[X(t)] \tag{17}$$

$$R(s) = E[(X(t)-\mu)(X(t+s)-\mu)] \tag{18}$$

$$\rho(s) = \frac{R(s)}{R(0)} \tag{19}$$

It can be shown that the power spectral density $S(\omega)$ is the Fourier Transform of the autocovariance function $R(s)$

$$S(\omega) = \frac{1}{2\pi}\int_{-\infty}^{\infty} R(s)e^{-i\omega s}ds\ . \tag{20}$$

This result gives necessary conditions to the existence of the spectrum: The autocovariance function $R(s)$ of $X(t)$ should have a Fourier Transform. It is interesting to note that the inverse Fourier Transform gives in particular

$$R(0) = \sigma^2 = \int_{-\infty}^{\infty} S(\omega)\,d\omega\ . \tag{21}$$

The variance σ^2 is equal to the total area of the spectrum.

Because it is not possible to completely define the stochastic process and its density function, we are then facing the problem of estimating the moments of the stochastic process. A solution to this problem is possible with the help of statistical analysis.

A.2 Statistical analysis tools

To simplify the symbols, we will only use X_t when refering to a single realization x_t or to the random variable X_t. It should be clear from the context whether we are discussing a particular set of numerical values or whether we are refering to a set of random variables.

Let $\{X(t)\}$ be a stationary process involving discrete realizations with mean μ, autocovariance $R(s)$, and autocorrelation $\rho(s)$. Given N observations $X_1, X_2 \ldots, X_N$, we define

$$\bar{X} = \frac{1}{N} \sum_{i=1}^{N} X_i \,. \tag{22}$$

We have, with the assumption of a stationary time series,

$$E[\bar{X}] = \frac{1}{N} \sum_{i=1}^{N} E[X_i] = \mu \tag{23}$$

$$var\{\bar{X}\} = \frac{\sigma^2}{N} \sum_{s=-(N-1)}^{N-1} (1 - \frac{|\, s \,|}{N}) \rho(s) \,. \tag{24}$$

If $E[\bar{X}]$ and $var\{\bar{X}\}$ are finite when $N \rightarrow \infty$, then $\bar{X}$ is said to be a consistent estimate of μ.

Using the same hypothesis, one can show that

$$\hat{R}(s) = \frac{1}{N} \sum_{i=1}^{N-|s|} (X_i - \bar{X})(X_{i+|s|} - \bar{X}) \tag{25}$$

is a biased estimate of the autocovariance function $R(s)$ but asymptotically consistent, and

$$\hat{\rho}(s) = \frac{\hat{R}(s)}{\hat{R}(0)} \tag{26}$$

is an asymptotically consistent estimate of the autocorrelation function $\rho(s)$.

The fundamental relationship (20) will lead us to consider an estimate $\hat{S}(\omega)$ which should be a Fourier Transform of the estimate $\hat{R}(s)$ of $R(s)$. However, it appears that this estimate is not consistent and not valid.
But, with a suitable lag window $\lambda_N(s)$, the new estimate

$$\hat{S}(\omega) = \frac{1}{2\pi} \sum_{s=-(N-1)}^{N-1} \lambda_N(s)\, \hat{R}(s)\, e^{-is\omega} \tag{27}$$

is consistent if $\lambda_N(s)$ has well suited properties, as for example the Tukey-Hanning lag window

$$\begin{aligned} \lambda_N(s) &= \frac{1}{2}(1+\cos\frac{\pi s}{M}) \qquad s \leq M \\ \lambda_N(s) &= 0 \qquad\qquad\qquad\quad s > M. \end{aligned}$$

with the window parameter M. It is possible to compute the estimate $\hat{S}(\omega)$ from the periodogram

$$I_N(\theta) = \frac{1}{2\pi N} \mid \sum_{s=-(N-1)}^{N-1} X(s)\, e^{-is\theta} \mid^2 \tag{28}$$

and

$$\hat{S}(\omega) = \int_{-\pi}^{\pi} I_N(\theta) W_N(\omega-\theta)\, d\theta \tag{29}$$

$$W_N(\omega) = \frac{1}{2\pi} \sum_{s=-(N-1)}^{N-1} \lambda_N(s)\, e^{-is\omega}\,. \tag{30}$$

A.3 Precision of spectral estimates

In practice, we can calculate an estimation $\hat{S}(\omega)$ of the spectrum $S(\omega)$ with a time series of finite length. We introduce errors in the estimation of $S(\omega)$, which can be quantified at each frequency ω by the bias $b(\omega)$ and the variance $v^2(\omega)$

$$b(\omega) = E[\hat{S}(\omega)] - S(\omega) \tag{31}$$

$$v^2(\omega) = var\{\hat{S}(\omega)\} \tag{32}$$

One approach to estimate the precision of spectral estimates is to compute the "p% Gaussian range of percentage error" $\Delta_p(\omega)$, which is defined by

$$\Delta_p(\omega) = \gamma_p \frac{v(\omega)}{S(\omega)} + \frac{\mid b(\omega) \mid}{S(\omega)} \tag{33}$$

with γ_p, the two sided p% point of the standardized Gaussian normal distribution. The product $S(\omega) \times \Delta_p(\omega)$ may be regarded as an upper bound for a p% confidence interval for $S(\omega)$. Priestley shows that when one desires a p% confidence and a given bandwidth resolution B_h, then $\Delta_p(\omega)$ is bounded by

$$\Delta_p = \gamma_p \sqrt{\frac{I_w M}{N} + \frac{1}{6M^2}\left(\frac{B_w}{B_h}\right)^2} \tag{34}$$

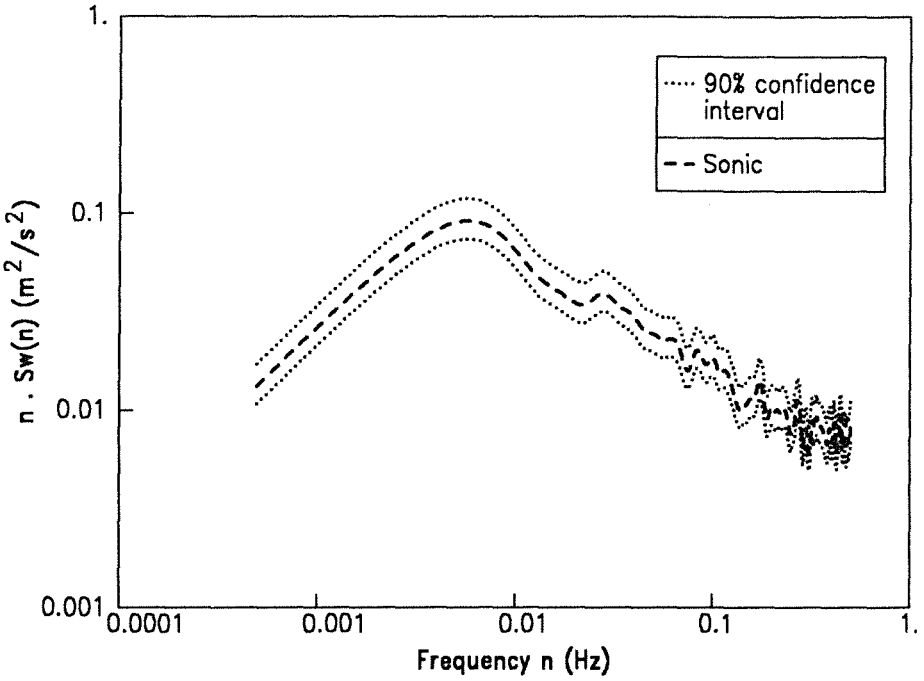

Figure 21: 90% confidence interval of sonic spectrum for run No 7.

with I_w and B_w, parameters depending on the window shape (see Priestley). We are then able to determine a confidence interval for the spectrum, written as

$$\frac{\hat{S}(\omega)}{1+\Delta_p} \leq S(\omega) \leq \frac{\hat{S}(\omega)}{1-\Delta_p} \,. \tag{35}$$

The strategy consists in calculating the M value that will minimize the error for a given time series. Priestley finds that, for a fixed record length N, one can choose

$$M = 3^{-2/5} \left(\frac{B_w^4}{I_w\, B_h^4}\right)^{1/5} N^{1/5}. \tag{36}$$

We have applied this procedure to the sonic data. During the run No 7, the fixed parameter is the number of points N (8225), the chosen parameters are (i) the Tukey-Hanning window ($B_w = 2.45\pi \ rad\, s^{-1}, I_w = 0.75$), (ii) the confidence interval 90% ($p = 0.90, \gamma_{0.9} = 1.96$), (iii) the bandwidth resolution B_h ($0.15 \ rad\, s^{-1}$). Then, $M = 97$ and $\Delta_{0.9} = 0.23$. Figure 21 illustrates this result. Because the number of observations and the spectrum bandwidth are nearly the same for the seven experiments, $\Delta_{0.9}$ only varies between 0.23 and 0.26, and M varies between 86 and 97.

B Spectral analysis with missing observations

Parzen (1963) and Bloomfield (1970) have discussed basic aspects of this theory. An excellent survey is given by Bloomfield from which we borrow freely.

Generally, the vertical velocity time series $W(t)$ does not have a zero mean value $\bar{W}$. If $\bar{W}$ is removed from the $W(t)$, a new time series $X(t)$ with zero mean is defined. It is considered to be stationary and to be defined at equally spaced intervals of time. The really measured amplitude modulated series, $Z(t)$ is constructed by replacing missing observations in the original $X(t)$ by their mean value zero. Thus,

$Z(t) = X(t)$ if observed.

$Z(t) = 0$ otherwise.

The amplitude modulation function $g(t)$ satisfies

$g(t) = 1$ if $X(t)$ is observed.

$g(t) = 0$ otherwise.

B.1 Amplitude modulation process

The amplitude modulation function $g(t)$ is assumed to be independent of $X(t)$. Then, we define β, $R_g(s)$ and the characteristic function $h(s)$ of the sampling scheme $g(t)$ by

$$\beta = E[g(t)] \tag{37}$$

$$R_g(s) = E[g(t)g(t+s)] \tag{38}$$

$$h(s) = R_g(s)/\beta\,. \tag{39}$$

The index g refers to the sampling scheme. One should note that β is the fraction of number of observed points to the observation time interval in seconds. Bloomfield imposed two conditions to the amplitude modulation function. He shows that its hypothesis are verified if

$$h(s) > 0 \qquad s = 0, \pm 1, \ldots \tag{40}$$

$$\sum_{s=-\infty}^{\infty} \mid h(s) - \beta \mid < +\infty\,. \tag{41}$$

Following Bloomfield, we find that

$$cov\{g(t), g(t+s)\} \to 0 \quad \text{, if} \quad s \to \pm\infty\,.$$

Thus, situations where $g(t)$ has some periodic component are not solved by this method. Jones (1962), Parzen (1962), Scheinok (1965) , Neave (1970),

Brillinger (1972), (1983) and Marsy (1978) have proposed solutions to specific situations including periodic missing data.

The amplitude modulated process $Z(t)$ follows the properties:

$$E[Z(t)] = 0 \tag{42}$$

$$R_z(s) = R_g(s) \times R_x(s) \tag{43}$$

with $R_z(s)$ and $R_x(s)$ the autocovariance of $Z(t)$ and $X(t)$.

The first consequence of these assumptions is that we are able to estimate the autocorrelation and autocovariance of $X(t)$ with these equations. We can compute the Fourier Transform of

$$c_g(s) = \beta^{-2} cov\{g(t), g(t+s)\}$$

under Bloomfield's assumption :

$$A(\omega) = \frac{1}{2\pi} \sum_{s=-(N-1)}^{N-1} c_g(s)\, e^{-is\omega} . \tag{44}$$

As a consequence, $S_z(\omega)$ can be written

$$S_z(\omega) = \beta^2 \left[S_x(\omega) + \int_{-\pi}^{\pi} A(\omega - \theta) S_x(\theta)\, d\theta \right] . \tag{45}$$

This is the key formula presented in Section 4. A solution of this equation can be found. Let us define

$$d_g(s) = \frac{1}{\beta}\left(\frac{1}{\beta} - \frac{1}{h(s)}\right) = \frac{c_g(s)}{R_g(s)} .$$

It can be proven that $d_g(s)$ is finite for each s and that its Fourier Transform $D_g(\omega)$ is continuous and bounded.

Then

$$S_x(\omega) = \beta^{-2}\, S_z(\omega) - \int_{-\pi}^{\pi} D_g(\omega - \theta) S_z(\theta)\, d\theta \tag{46}$$

or with the notation $\Gamma(\omega) = \beta^2\, D_g(\omega)$,

$$S_x(\omega) = \beta^{-2} \left[S_z(\omega) - \int_{-\pi}^{\pi} \Gamma(\omega - \theta) S_z(\theta)\, d\theta \right] . \tag{47}$$

This notation is similar to the formulation of the solution of continuous time series spectral estimates with random sampling (Marsy, 1978).

B.2 Estimate of $S_x(\omega)$

Throughout this section, the basic assumptions are those stated in section B.1. These assumptions will be demonstrated in section B.3. To calculate an estimate of $S_x(\omega)$, we use the method of moments: The estimators $\hat{\Gamma}(\omega)$, $\hat{\beta}$, $\hat{R}_g(s)$ are supposed to have the exact values of $\Gamma(\omega)$, β, $R_g(s)$. The estimates bias and variance of the time series $Z(t)$ are calculated following the basic approach (Appendix A).
Then, we define

$$\hat{S}_x(\omega) = \beta^{-2}\left[\hat{S}_z(\omega) - \int_{-\pi}^{\pi} \Gamma(\omega-\theta)\hat{S}_z(\theta)\,d\theta\right] \tag{48}$$

which can be written in a similar form as Eq.(27)

$$\hat{S}_x(\omega) = \frac{1}{2\pi}\sum_{s=-(N-1)}^{N-1} \frac{\hat{R}_z(s)}{R_g(s)}\lambda_N(s)\; e^{-is\omega}\;. \tag{49}$$

Eq. (49) is more convenient for computation. Following Priestley (1981) and Marsy (1976), we can show that this estimate is asymptotically consistent. The bias is expressed by

$$b_x(\omega) = E[\hat{S}_x(\omega)] - S_x(\omega) = \frac{1}{2}S_x''(\omega)\int_{-\pi}^{\pi}\theta^2 W_N(\theta)\,d\theta. \tag{50}$$

with the prime indicating frequency derivation. Priestley shows that, when using Tukey-Hanning windows, the bias can be expressed as:

$$b_x(\omega) = \frac{1}{6M^2}\left(\frac{B_w}{B_h}\right)^2 S_x(\omega). \tag{51}$$

As mentioned by Bloomfield, the variance is, with Priestley's notation,

$$var\{\hat{S}_x(\omega)\} = \frac{M}{N}S_z^2(\omega)\,\frac{I_w}{\beta^4}\,(1+\delta_{\omega,0,\pi})\;. \tag{52}$$

with Kronecker's symbol $\delta_{\omega,0,\pi}$ being 1 for $\omega = 0, \pm\pi$, and being 0 otherwise. Following Eq.(33) and Priestley, we have

$$P\Big[\mid \hat{S}_x(\omega) - S_x(\omega)\mid \leq \Delta_p(\omega)\,S_x(\omega)\Big] \geq \frac{p}{100}, \tag{53}$$

with $P\Big[\;\Big]$ indicating the probability function. Then,

$$\mid \hat{S}_x(\omega) - S_x(\omega)\mid_p \leq \mid b_x(\omega)\mid + \gamma_p\, var\{\hat{S}_x(\omega)\}^{1/2}. \tag{54}$$

Index p is indicating that this relationship is true with a probability of p%. For ω not equal to 0, $\pm\pi$, and following Eqs.(52) and (54)

$$\mid \hat{S}_x(\omega) - S_x(\omega)\mid_p \leq \mid b_x(\omega)\mid + \gamma_p\,\frac{M}{N}S_z^2(\omega)\,\frac{I_w}{\beta^4}. \tag{55}$$

In this case, it is not possible to calculate a simple confidence interval as in Appendix A.3 because $S_z(\omega)$ and $S''_x(\omega)$ are independant. It is necessary to estimate the spectrum $S_z(\omega)$ and the spectrum $S''_x(\omega)$ using two different confidence intervals. The real confidence interval of $\hat{S}_x(\omega)$ is then based on the intersection of the two confidence intervals. The study of the estimate of $S_x(\omega)$ is then separated in two parts, the first one dealing with $S''_x(\omega)$ and the bias $b_x(\omega)$, the second one dealing with the spectrum $S_z(\omega)$ and the variance $var\{\hat{S}_x(\omega)\}$.

Results of the computation of the confidence intervals of the sonic spectra indicate that the bias corresponds to less than 20% of the total percentage error. We suppose that, in the frequency band not perturbated by the missing data (below 0.05 Hz), the percentage error of the SODAR spectra is of the same order as in the case of the sonic spectra. The bias and variance introduced by the missing data are not greatly increasing the total error, as suggested by the Figures presented in Section 4. However, in the frequency band pertubated by missing data (frequencies above 0.05 Hz), the bias is very important when the power spectrum is greatly underestimated. In this case, the hypothesis is no more valid; we also know that the power spectrum has no sense any more. Then, in the frequency band not greatly perturbated by the missing data, we assume

$$| b_x(\omega) | \ll \gamma_p var\{\hat{S}_x(\omega)\}^{1/2}.$$

Considering this hypothesis and Eq.(54), we have (asymptotically) with p% confidence,

$$| S_x(\omega) - \hat{S}_x(\omega) |_p \leq \gamma_p var\{\hat{S}_x(\omega)\}^{1/2} \tag{56}$$

giving

$$S_x(\omega) \leq \hat{S}_x(\omega) + \gamma_p var\{\hat{S}_x(\omega)\}^{1/2} . \tag{57}$$

and, following Eq.(51),

$$| b_x(\omega) |_p \leq \frac{1}{6M^2}(\hat{S}_x(\omega) + \gamma_p var\{\hat{S}_x(\omega)\}^{1/2})\left(\frac{B_w}{B_h}\right)^2. \tag{58}$$

Concerning the spectrum $S_z(\omega)$, the results of Section A.3 are applicable, because there is no missing data for the random variable $Z(t)$. We have then, following Eq.(35),

$$| S_z(\omega) |_{p'} \leq \frac{\hat{S}_z(\omega)}{1 - \Delta_{p'}} . \tag{59}$$

with $\Delta_{p'}$, the p'% Gaussian range of percentage error of $S_z(\omega)$ calculated following the results of Appendix A. $\Delta_{p'}$ has the same value as in the case of the sonic data because there is no missing data for the random variable $Z(t)$. Then, following Eqs.(52) and (59)

$$var\{\hat{S}_x(\omega)\} \leq \frac{M I_w}{N\beta^4}\left(\frac{1}{1 - \Delta_{p'}}\right)^2 \hat{S}_z^2(\omega). \tag{60}$$

Now, we are able to calculate a confidence interval for $\hat{S}_x(\omega)$. Following Eq.(58) and Eq.(60), we obtain

$$| S_x(\omega) - \hat{S}_x(\omega) |_{p \times p'} \leq \frac{1}{6M^2} \hat{S}_x(\omega) \Big(\frac{B_w}{B_h}\Big)^2 + \Big[\frac{1}{6M^2}\Big(\frac{B_w}{B_h}\Big)^2 \gamma_p + \gamma_p\Big] var\{\hat{S}_x(\omega)\}^{1/2}$$

Furthermore, using $p = p'$, $\gamma_p = \gamma_{p'}$ and having

$$\frac{1}{6M^2}\Big(\frac{B_w}{B_h}\Big)^2 \ll 1$$

with $M \approx 100$, $B_h \approx 0.15\ rad\, s^{-1}$, $B_w = 2.45\pi\ rad\, s^{-1}$, we obtain

$$| S_x(\omega) - \hat{S}_x(\omega) |_{p \times p'} \leq \frac{1}{6M^2} \hat{S}_x(\omega) \Big(\frac{B_w}{B_h}\Big)^2 + \gamma_p var\{\hat{S}_x(\omega)\}^{1/2} \qquad (61)$$

Then, following Eq.(60) and Eq.(61),

$$| S_x(\omega) - \hat{S}_x(\omega) |_{p \times p'} \leq \gamma_p \frac{1}{\beta^2} \frac{1}{1 - \Delta_{p'}} \sqrt{\frac{I_w M}{N}}\, \hat{S}_z(\omega) + \frac{1}{6M^2}\Big(\frac{B_w}{B_h}\Big)^2 \hat{S}_x(\omega). \qquad (62)$$

Following Eq.(48) and the experimental results, the convolution of Γ and $\hat{S}_z(\omega)$ should have a small influence on $\hat{S}_x(\omega)$ for frequencies below 0.05 Hz. In this case, $\hat{S}_x(\omega) \approx \beta^{-2}\, \hat{S}_z(\omega)$. Then for $p = p' = 0.9$,

$$\gamma_p \frac{1}{1 - \Delta_{p'}} \sqrt{\frac{I_w M}{N}} \approx 0.28 \qquad (63)$$

$$\frac{1}{6M^2}\Big(\frac{B_w}{B_h}\Big)^2 \approx 0.05\ . \qquad (64)$$

The bias expressed by the second relationship is about 18% of the error introduced by variance and expressed by the first relationship.

The following Figures 22 to 28 illustrate the results of Eq.(62) for the seven runs. The chosen parameters and the truncation value of the Tukey–Hanning spectral window are the same as for the confidence intervals of the sonic spectra.

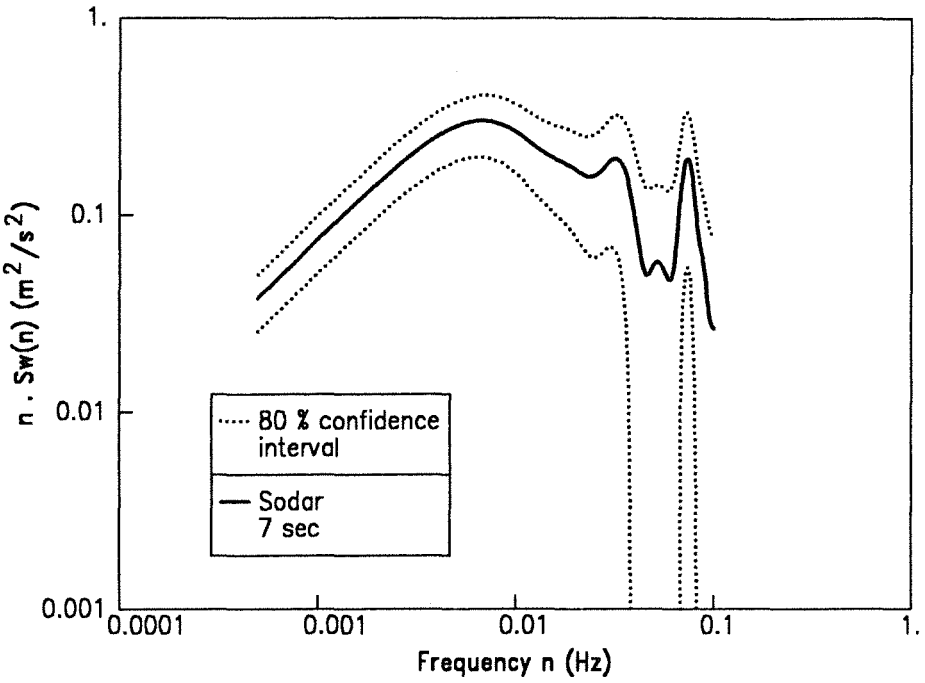

Figure 22: 80% confidence interval of SODAR data. Run No 1 (01/08/90).

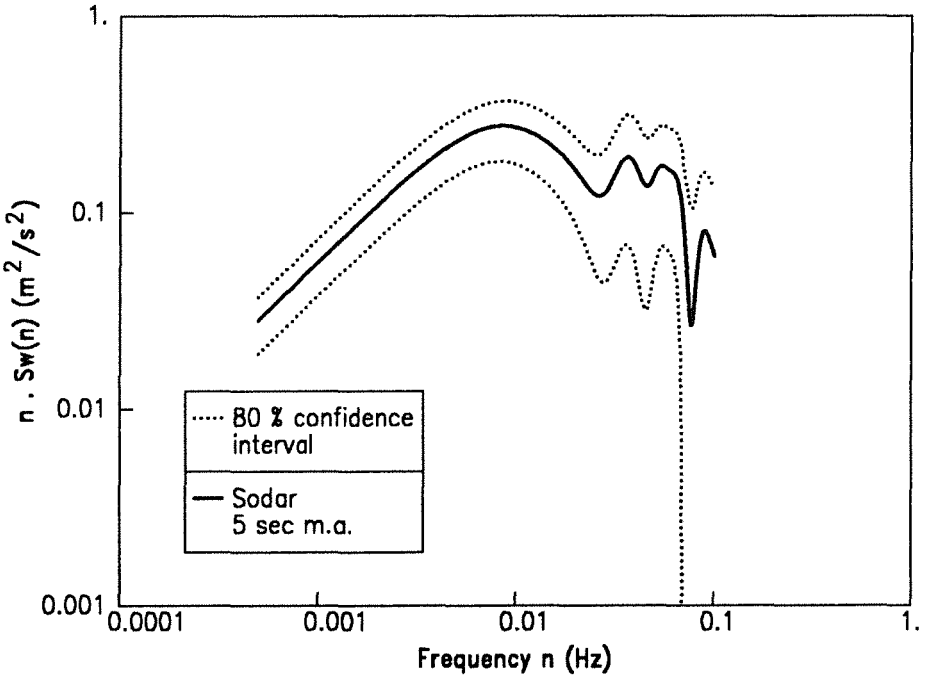

Figure 23: 80% confidence interval of SODAR data. Run No 2 (10/08/90).

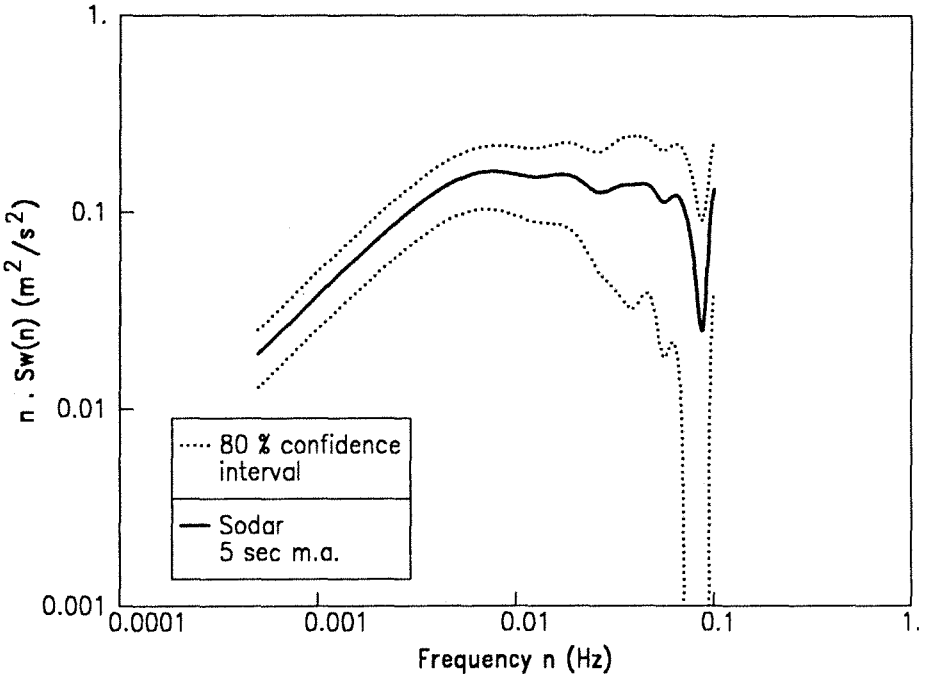

Figure 24: 80% confidence interval of SODAR data. Run No 3 (15/08/90).

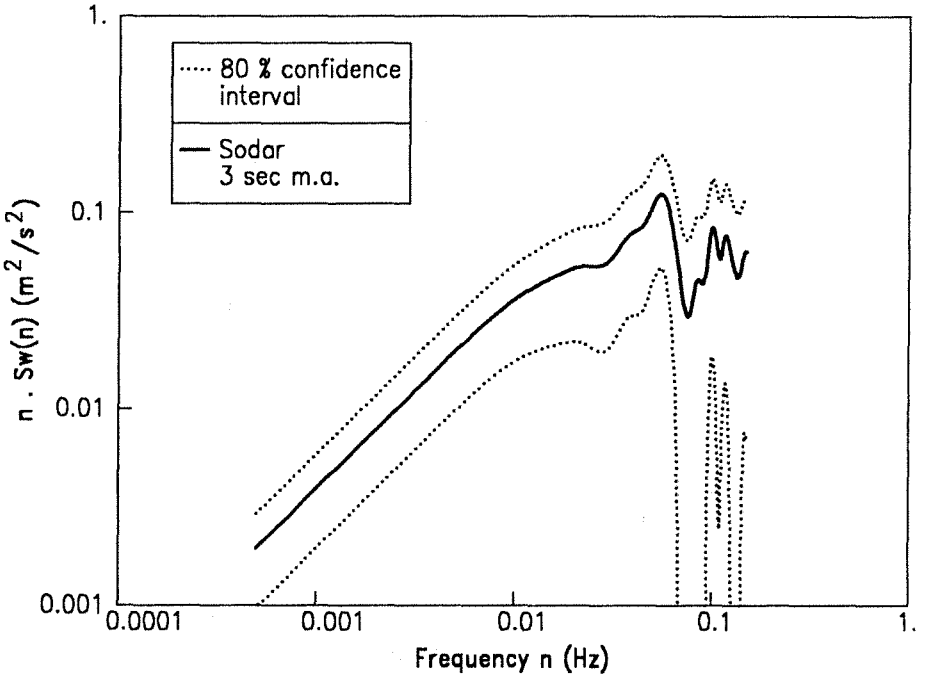

Figure 25: 80% confidence interval of SODAR data. Run No 4 (16/08/90).

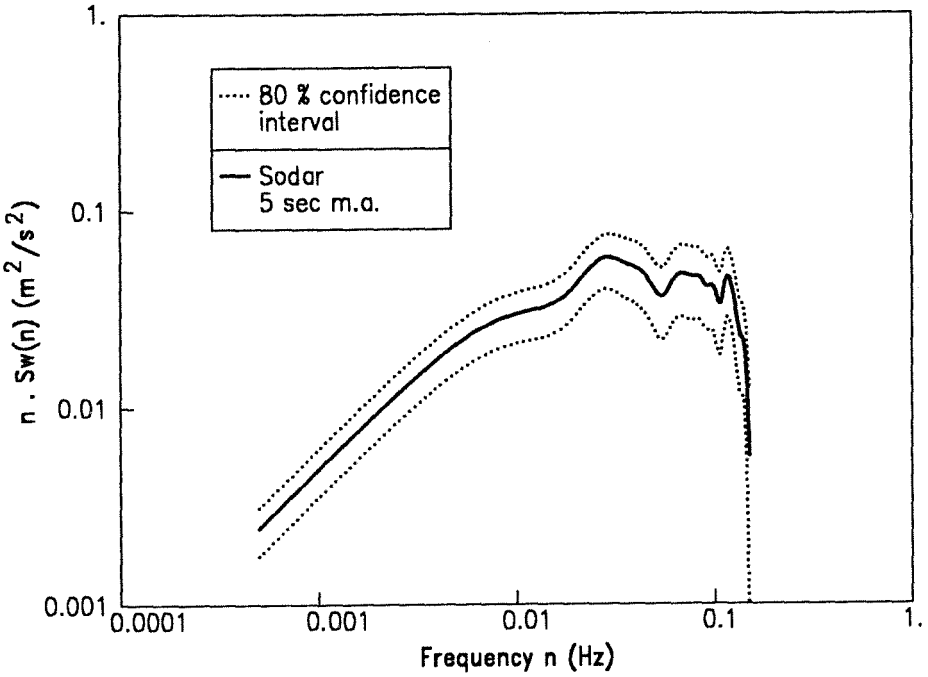

Figure 26: 80% confidence interval of SODAR data. Run No 5 (04/09/90).

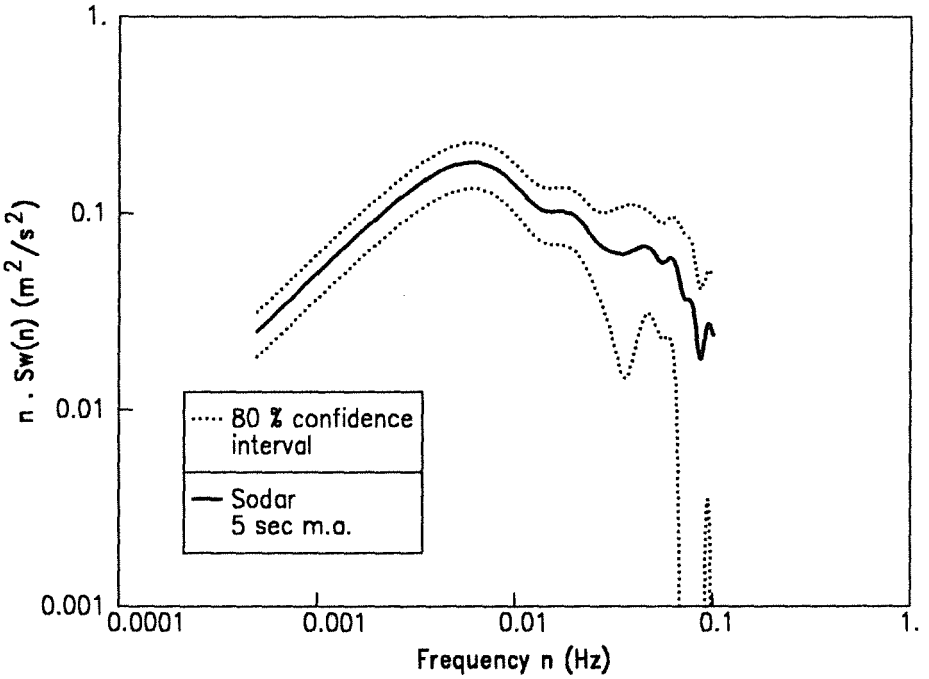

Figure 27: 80% confidence interval of SODAR data. Run No 6 (05/09/90).

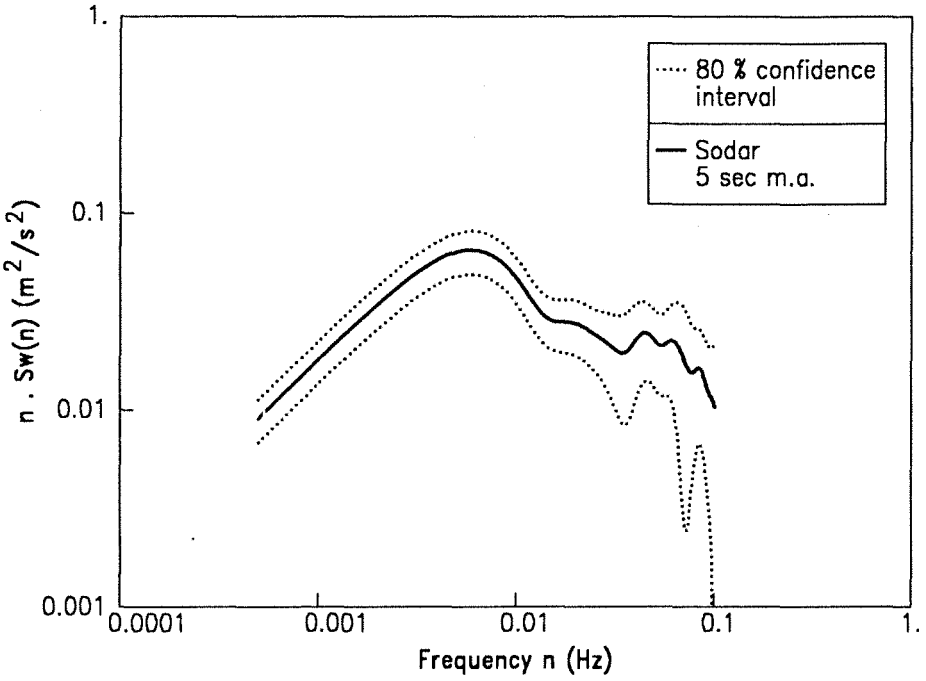

Figure 28: 80% confidence interval of SODAR data. Run No 7 (11/09/90).

B.3 Comments about the assumption of Bloomfield theory

Instead of a periodic sampling with randomly missing data, the sampling scheme can represent a renewal process (Bloomfield). In this case, the intervals between successive observations are independent random variables, each with β, being the fraction of the observed points to the time duration in seconds and probability function $f_n(t)$, which is the density function of the time interval between samplings at times t_{k+n} and t_k for all k ($f_1(t)$ is depicted for the run No 5 in Figure 5, section 4.1.2). Bloomfield shows for $h(s)$ of Eq.(39):

$$h(s) > 0 \qquad \text{for all s}$$
$$h(s) \to \beta \qquad \text{if} \qquad s \to \pm\infty.$$

if $f_1(t) > 0$ for all t. Figure 29 illustrates the function $h(s)$ for run No 6. The small peaks represent the 27 s cycles. With increasing lags, the magnitude of the peaks decreases slowly, and therefore the characteristic function $h(s)$ tends to a finite limit. This is in fair agreement with the theory of a renewal process.

Figure 30 shows how $h(s)$ evolves with increasing averaging width (see Appendix C). The overall shape of the function remains the same for original data or smoothed data, but the small "high frequencies" variations are filtered.

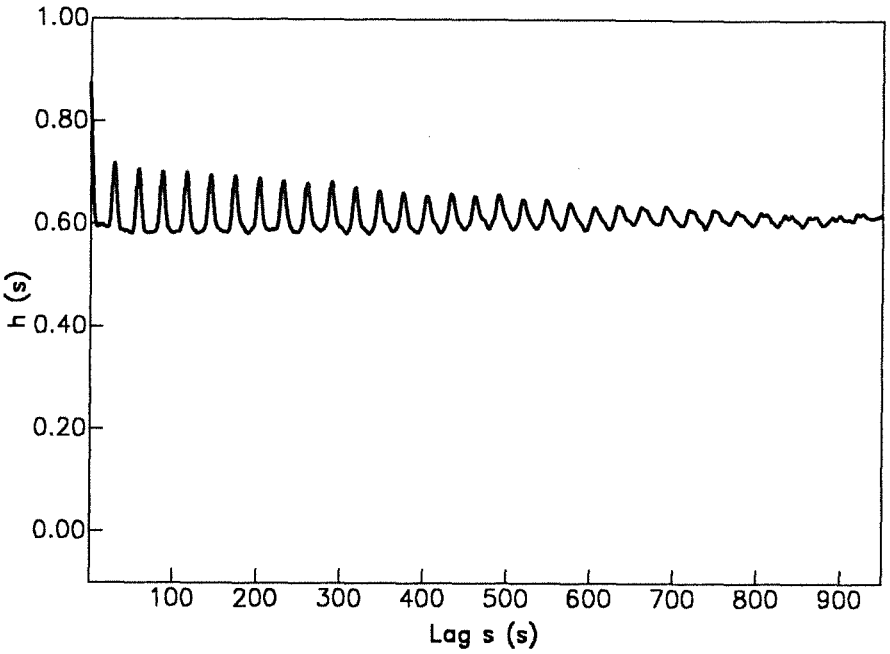

Figure 29: Characteristic function of the sampling scheme, run No 6.

One condition under which the Bloomfield hypothesis is completely valid is Eq.(41). Figure 31 shows a particular example of $\mid h(s) - \beta \mid$. This decreasing function suggests that it is bounded by a decreasing exponential function, integrable over $[0, +\infty)$. Then, it follows that Bloomfield's hypothesis is valid for run No 6. All the other runs suggest that this is generally applicable for the SODAR sampling scheme.

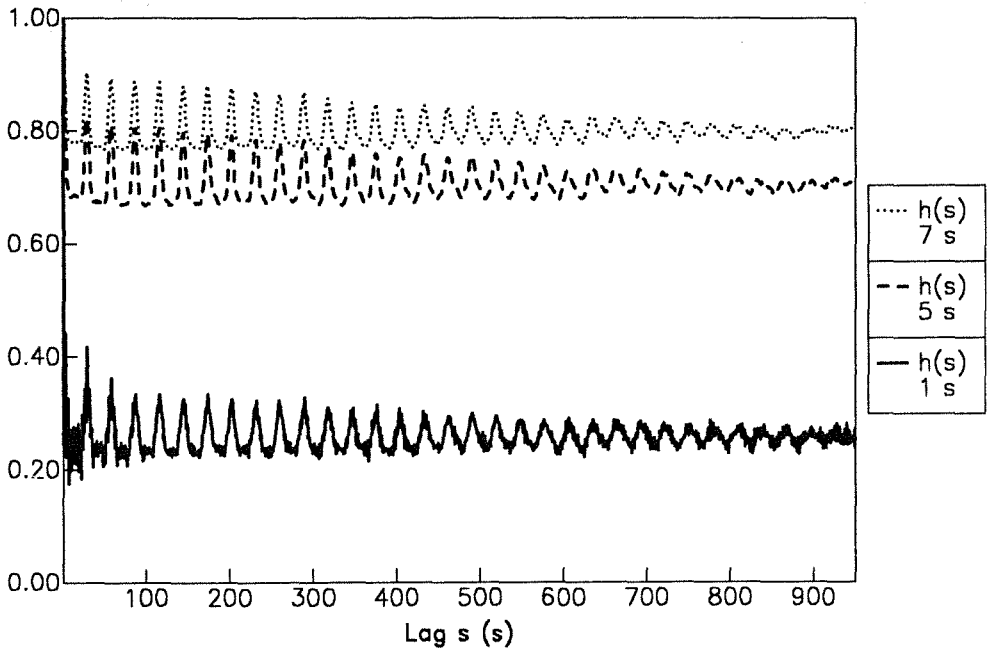

Figure 30: Evolution of the characteristic function with averaging time.

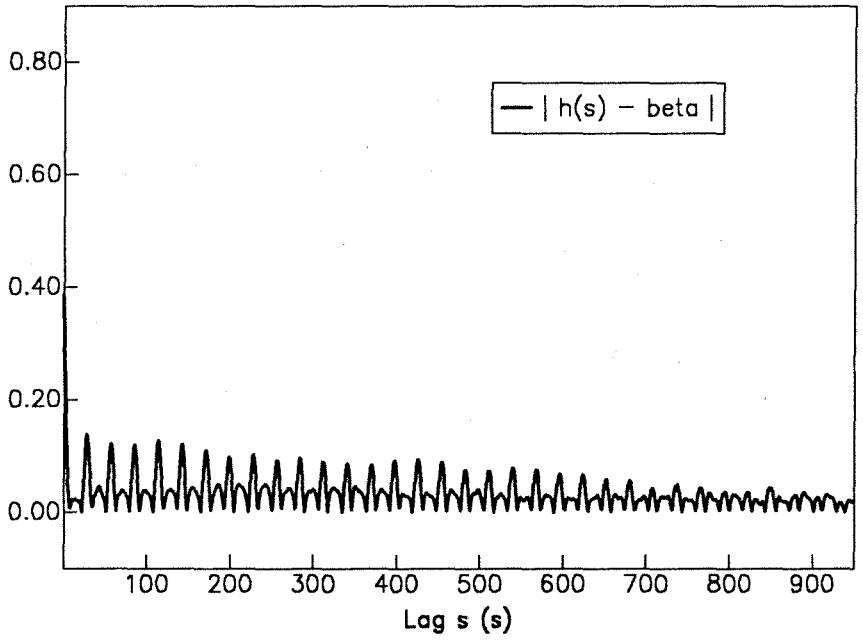

Figure 31: Properties of the characteristic function, run No 6.

C Moving average procedure

The purpose of the moving average procedure is to increase the percentage of "observed" data and to randomize the spectral functions $A(\omega)$ and $\Gamma(\omega)$, representing the sampling scheme properties (see Eqs.(42) and (47). We can summarize the properties of this data transformation in two points:

(i) This process is a low-pass filter which has some influence on the spectrum . A demonstration of this undesired effect is presented in Figure 32.

(ii) This averaging procedure reduces the undesired peaks of the functions $A(\omega)$ and $\Gamma(\omega)$.

C.1 Characteristics of the low-pass filtering procedure

Following conventional descriptions, we consider in this section the stationary time series $X(t)$ as the input and the transformed time series $Y(t)$ as the output of a linear filter. The output time series is defined by

$$Y(s) = \sum_{k=-m}^{m} a_k X(k+s) \tag{65}$$

$$a_k = \frac{w_k}{\bar{w}} \tag{66}$$

$$\bar{w} = \sum_{k=-m}^{m} w_k \tag{67}$$

with chosen weights w_k. The transfer function of the filter is then,

$$H(\omega) = \sum_{k=-m}^{m} a_k e^{-i\omega k} \tag{68}$$

Since, in general, $H(\omega)$ is complex we may write it in the form

$$H(\omega) = G(\omega)\, exp(i\phi(\omega)), \tag{69}$$

with $G(\omega)$ called the gain at frequency ω, and $\phi(\omega)$ called the phase-shift at frequency ω. We then obtain, following the above arguments,

$$\mid H(\omega) \mid^2 = \frac{S_Y(\omega)}{S_X(\omega)}, \tag{70}$$

with $S_X(\omega)$ and $S_Y(\omega)$ being spectra of the time series. We denote n_c as the cutoff frequency corresponding to half power, i.e. $\mid H(n_c) \mid^2 = 0.5$.

Equal-weight or arithmetic averaging consists in giving the same weight to all values $w_k = 1/(2m+1)$. It is easy to show that the transfer function in this case is

$$H(n) = \frac{1}{2m+1} \frac{\sin(2m+1)\pi n}{\sin \pi n}.$$

The phase-shift of this filter is in theory equal to 0 or π, because the filter is symmetric. Following Jones(1972), we did not choose this simple averaging procedure, but instead used the Cressman weight function

$$w_k = \frac{(m+1)^2 - k^2}{(m+1)^2 + k^2}$$

which has also the particularity to have a phase-shift equal to 0 or π. An interesting feature of the following Figure 32 is the difference between the arithmetic and Cressman low pass filters: The equal weight gain function decreases more quickly.

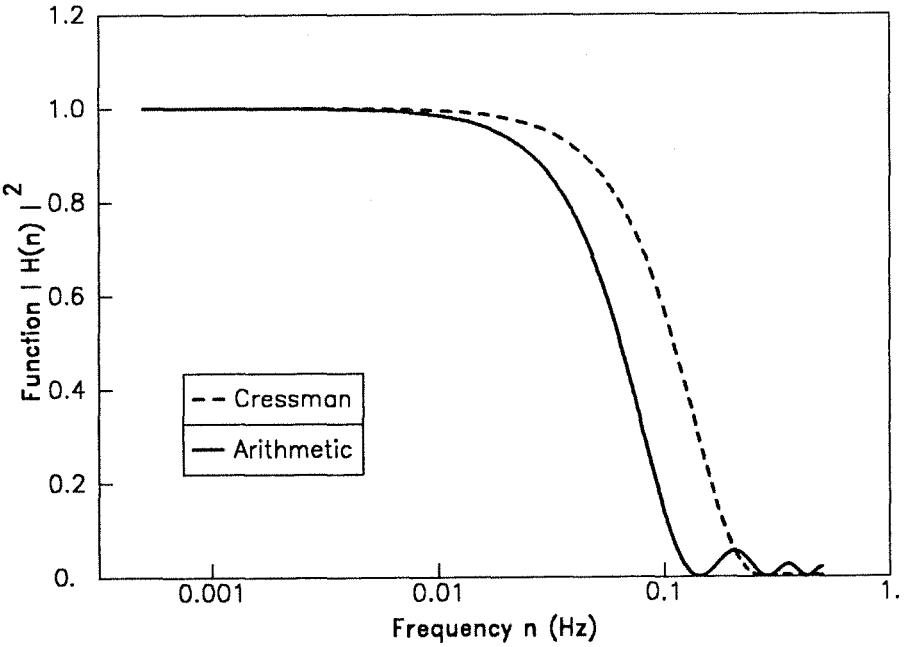

Figure 32: Comparison of Cressman and arithmetic low-pass filters.

We have applied this filtering procedure to the sonic data. Spectra of filtered and unfiltered data were computed with the same window parameter M. The effective transfer function, i.e. the ratio between the filtered and unfiltered spectra, is presented in Figure 33. The cutoff frequencies n_c for 3, 5, and 7 s averaging intervals are respectively 0.173 Hz, 0.11 Hz, and 0.0815 Hz. The phase-shifts calculated with sonic data are shown in Figure 34 for the different averaging widths.

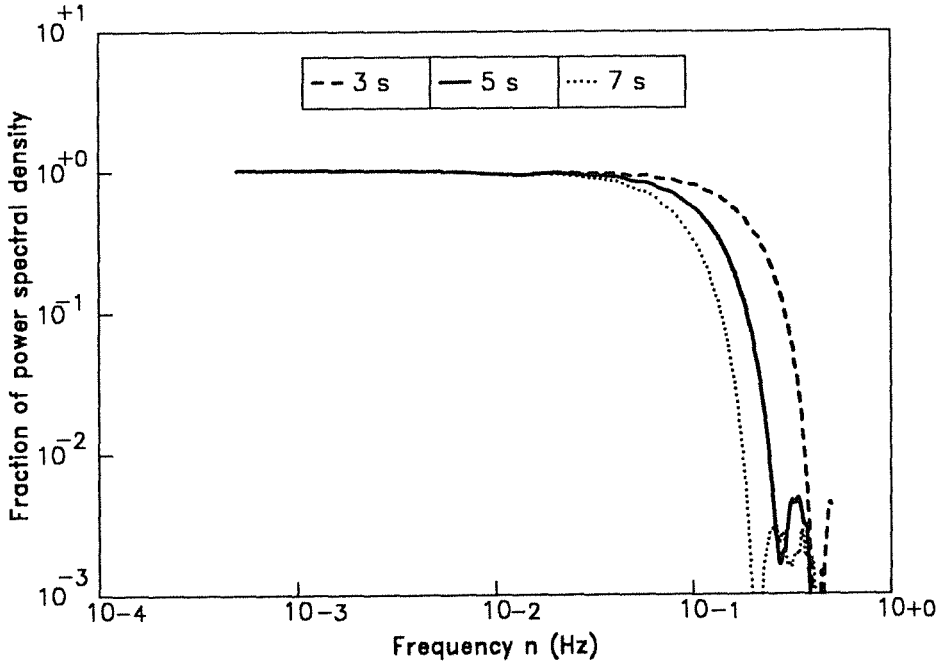

Figure 33: Fraction of power specral density $S_Y(\omega)/S_X(\omega)$ with Cressman weigthing of 3, 5, and 7 s averaging width applied to sonic data.

Examination of Figures 33 and 34 reveals that only in the frequency band $n \leq n_c$, where $H(n)$ is close to 1 and the phase shift ϕ is close to 0, this procedure is meaningful. With a 3, 5, or 7 s averaging interval, this is the case for a frequency band below 0.05 Hz.

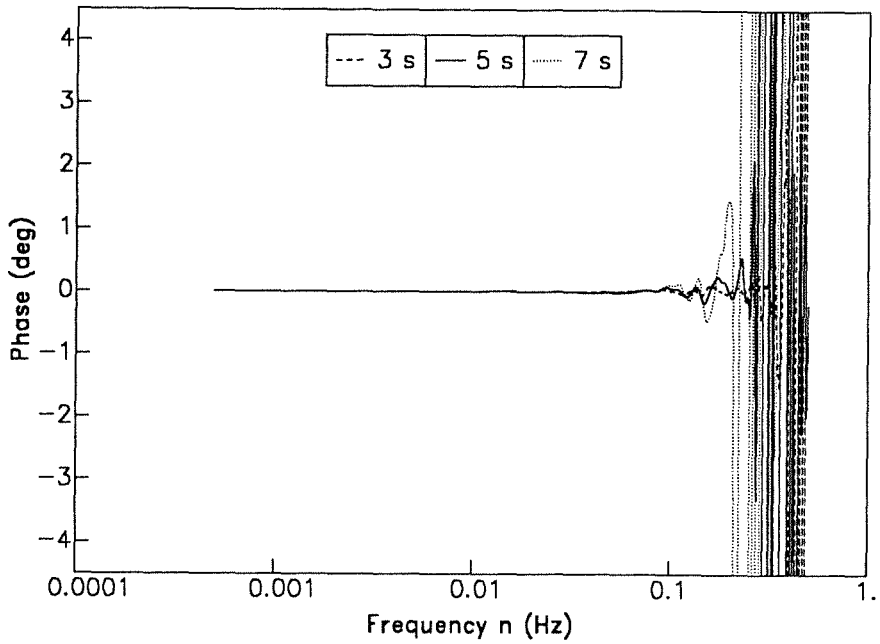

Figure 34: Phase-shift of Cressman filter with 3, 5, and 7 s averaging width applied to sonic data.

C.2 Influence of the low-pass filtering procedure on SODAR spectra

With the notation of section B, we study the evolution of the parameter β and the shape of $A(\omega)$ and $\Gamma(\omega)$. The weights are applied to the time series $Z(t)$. Table 8 shows the evolution of β with increasing averaging widhts.

Table 8: Influence of averaging interval on ratio β of availabe data for run No 1.

Lag m	0	1	2	3	4
Averaging width (s)	**1**	**3**	**5**	**7**	**9**
β	0.11	0.28	0.38	0.46	0.53

The functions $\Gamma(\omega)$ and $A(\omega)$ have been computed for the same averaging intervals. As expected, the high peak at 0.04 Hz due to the periodic

calibrations is greatly reduced with increasing averaging intervals and β (see Figure 35).

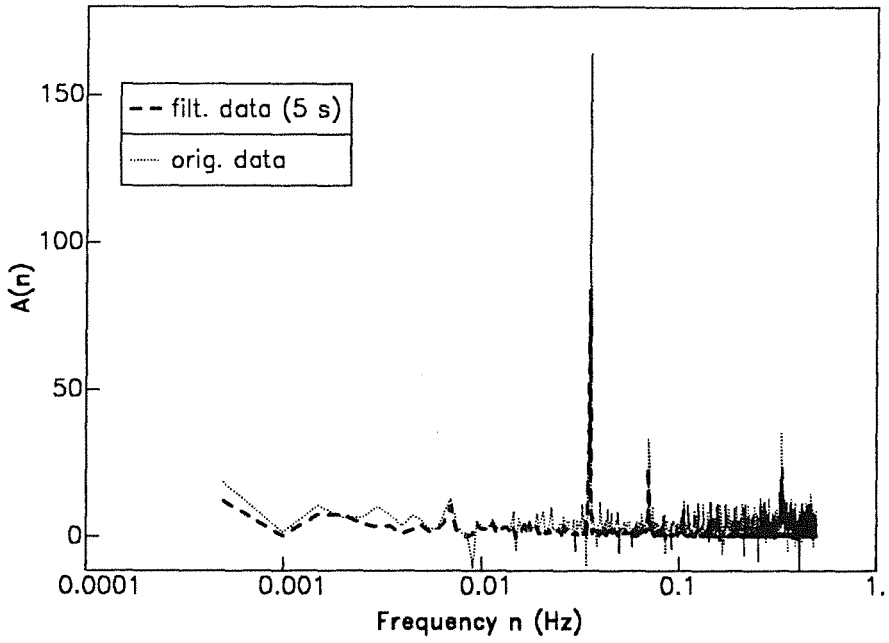

Figure 35: Function $A(\omega)$ for original data and filtered data with averaging interval of 5 s, run No 6.

We have compared the functions $A(\omega)$ calculated for runs No 2, 6, and 7, which have roughly 50%, 60%, and 70% of data available (see Figure 36). Apparently, there is no great difference of $A(\omega)$ at the frequency peak corresponding to the periodic calibration when $\beta \geq 0.5$. Therefore, there is no need to increase the averaging interval beyond 7 s.

Figure 37 represents an example of the effect of the moving average procedure. Although the spectrum derived from original data is inaccurate for frequencies above 0.03 Hz with two typical nadirs at 0.03 Hz and 0.09 Hz, the spectrum derived from transformed data is consistent for frequencies up to 0.07 Hz. Summarizing the consequences of moving average on sampling: It has the desired properties of increasing β and reducing the intensity of peaks in the functions $\Gamma(\omega)$ and $A(\omega)$.

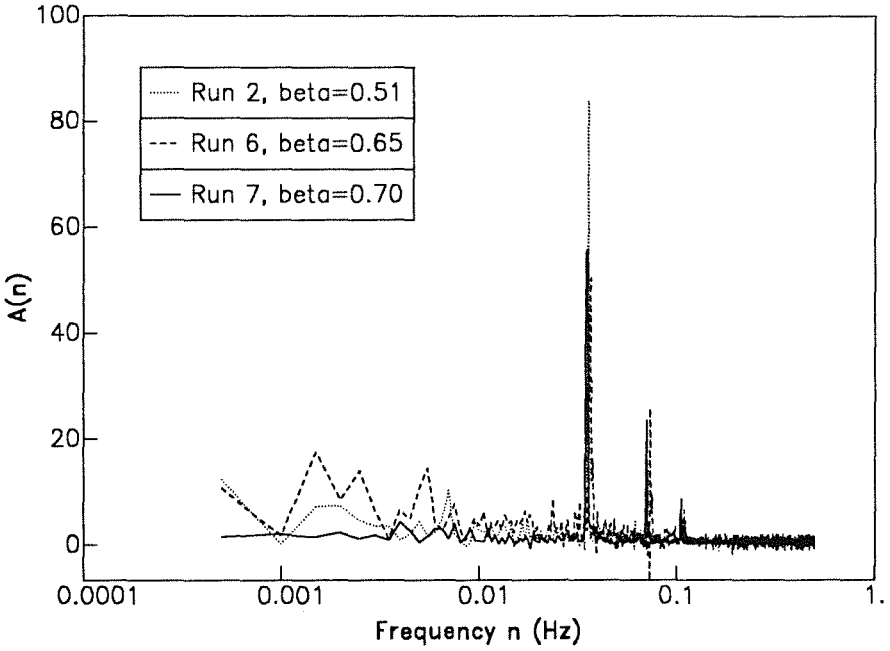

Figure 36: $A(\omega)$ for filtered data, runs No 2, 6, and 7.

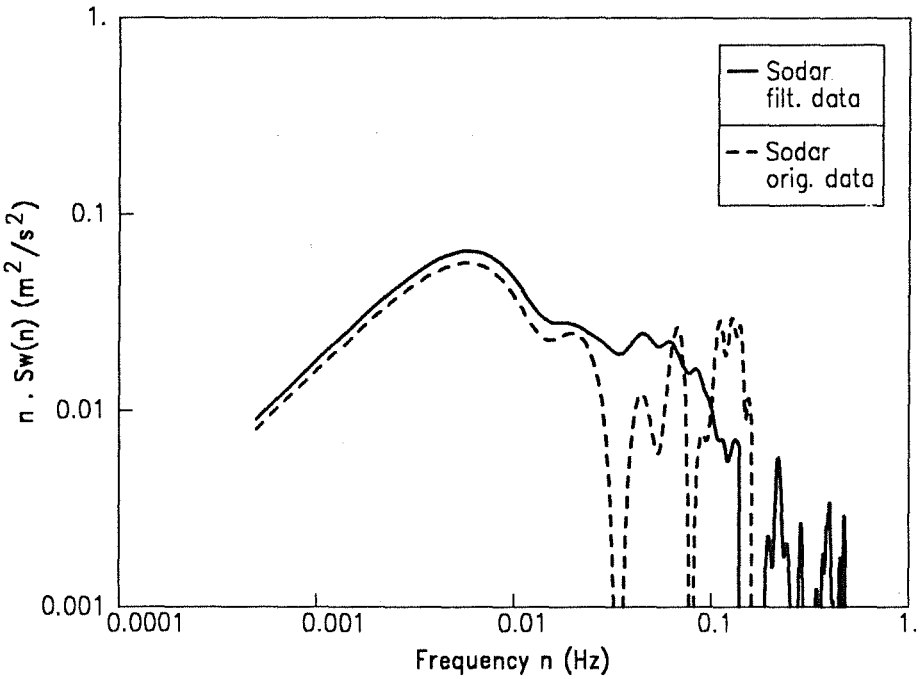

Figure 37: Comparison of spectra derived from original and filtered SODAR data, run No 7.

C.3 Sonic low-pass filter

The sonic data are observed at N equally spaced times t_1, t_2, t_3,...,t_N with a 1.06 s sampling rate. It is desired to smooth these data to obtain a 1 s sampling rate. Considering a time t situated between two values t_k and t_{k+1}, the chosen weights are compiled in Table 9 and plotted in Figure 38.

Table 9: Chosen weights $w_k/\bar{w}$ for the sonic low-pass filter.

Time t (s)	$w_k/\bar{w}$	$w_{k+1}/\bar{w}$
$t \leq t_k + 0.05$	1	0
$t_k + 0.05 \leq t \leq t_{k+1} - 0.05$	$\frac{(t-t_{k+1})^2}{(t-t_k)^2+(t-t_{k+1})^2}$	$\frac{(t-t_k)^2}{(t-t_k)^2+(t-t_{k+1})^2}$
$t \geq t_{k+1} - 0.05$	0	1

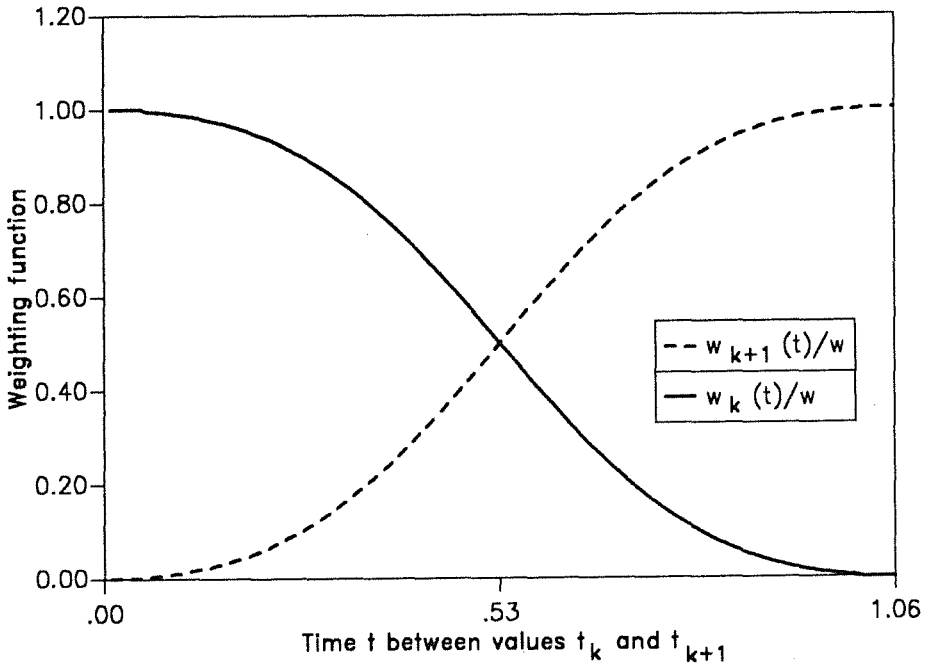

Figure 38: Weights of the sonic low-pass filter.

Figure 39 illustrates an example of filtered and unfiltered sonic spectra. The phase-shift in the band between 0.03 Hz and 0.5 Hz is due to this procedure. The filtered data show a $-2/3$ slope corresponding to the inertial subrange for frequencies up to 0.5 Hz, although the original data are contaminated by aliasing. Therefore, this filtering procedure is satisfactory.

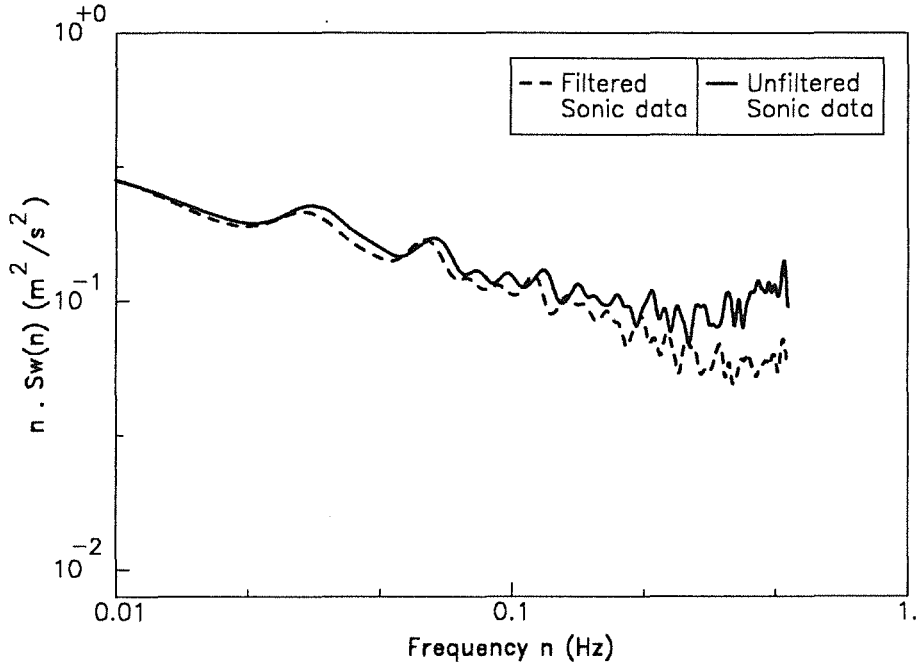

Figure 39: Comparison of sonic filtered and unfiltered data.

Acknowledgments

The authors thank Dr. N. Kalthoff for his helpful comments and his assistance when using the sonic anemometer. Mr. P. Burger participated fully in the experiments described. Mr. K.H. Pfeffer and Ms. S. Honcu helped in the data transfer and the data processing.

We are also grateful to Dr. G. Quinn and Dr. M.Tercel from KfK-IGT who helped in the redaction of the paper and the correction of the manuscript.

References

Arya S.P., 1988 : *Introduction to Micrometeorology.* International Geophysic Series, Vol 42, Academic Press, San Diego, California, USA.

Asimakopoulos D.N., Cole R.S., Crease B.A., Caughey S.J., 1978: *A comparison of Acoustic Doppler Vertical Velocity Power Spectra with Direct Measurements.* Atmos. Environ., Vol. 12, 1951-1956.

Bloomfield P. , 1970 : *Spectral Analysis with Randomly Missing Observations.* J. of Roy. Statist. Soc., Series B, Vol. 32, 369-380.

Brillinger D.R., 1972 : *The spectral analysis of stationary interval functions.* Proc. 6th Berkeley Symp. Prob. Statist., University of California Press, Berkeley, CA, 483-513.

Brillinger D.R., 1983 : *Statistical Inference for Irregularly observed processes.* Time Series Analysis of Irregularly Observed Data, Proc. of Symp., Lecture Notes in Statistics 25, 39-55.

Chintawongvanich P., Olsen R. and Biltoft C.A., 1989: *Intercomparison of Wind Measurements from Two Acoustic Doppler Sodars, a Laser Doppler Lidar, and In Situ Sensors.* J Atmos. Oceanic Technol., Vol. 6, 785-797.

Congeduti F., Fiocco G., Adriani A. and Guarrella C., 1981 : *Vertical Wind Velocity Measurements by a Doppler Lidar and Comparison with a Doppler Sodar.* Applied. Optics., Vol. 20, No. 12, 2048-2054.

Dilger H., 1976 : *Das meteorologische Meßsystem des Kernforschungszentrums Karlsruhe.* KfK 2347, KfK, Karlsruhe, FRG.

Dunsmuir W., Robinson P.M., 1981: *Asymptotic theory for time series containing missing and amplitude modulated observations.* Sankhya, Vol. 43, Series A, Pt 3, 260-281.

Frisch A.S. and Clifford S.F., 1974 : *A Study of Convection Capped by a Stable Layer using Doppler Radar and Acoustic Echo Sounders.* J. Atmos. Sci., Vol. 31, 1622-1628.

Gaynor J.E., 1977 : *Acoustic Doppler Measurement of Atmospheric Boundary Layer Velocity Structure Functions and Energy Dissipation Rates.* J. Appl. Meteor., Vol. 16, 148-155.

Hanufusa T., Fujitani T., Kobori Y., Mitsuta Y., 1982 : *A new type sonic anemometer-thermometer for field operation.* Pap. Meteorol. Geophys., Vol. 33, 1-19.

Helmis C.G., Asimakopoulos D.N. and Cole R.S. , 1985 : *A low level atmospheric vertical velocity comparison between a high-resolution acoustic sounder and a turbulence probe.* IEEE Trans. Geosc. and rem. sensing, Vol. GE-23, No. 2, 164-170.

Hinze J.O., 1959 : *Turbulence.* Mc Graw Hill Series in Mechanical Engineering, Mc Graw Hill, New. York.

von Holleuffer-Kypke R., Hübschmann W.G., Süß F ., Thomas P. (1984): *Meteorologisches Informationssystem des Kernforschungszentrums Karlsruhe.* Atomkernenergie, Kerntechnik Vol 44, No. 4, 300-304.

Jenkins G.M. and Watts D.G., 1968: *Spectral Analysis and Its Applications.* San Francisco, Holden-Day.

Jones R.H., 1962: *Spectral analysis with regularly missed observations.* Ann. Math. Statist., Vol. 33, 455-461.

Jones R.H., 1972: *Aliasing with Unequally Spaced Observations.* J. Appl. Met., Vol. 11, No. 2, 245-254.

Kaimal J.C., 1972: *Turbulence Spectra, Length Scale and Structure Parameters in the Stable Surface Layer.* Bound.-Layer Meteorol., Vol. 4, 289-309.

Kaimal J.C., Wyngaard J.C., Haugen D.A., Coté O.R. and Izumi Y., Caughey S.J. and Readings C.J., 1976: *Turbulence Structure in the Convective Boundary Layer .* J. Atmos. Sci., Vol. 33, 2152-2169.

Kaimal J.C., Gaynor J.E., Finkelstein P.L., Graves M.E. and Lockhart T.J., 1984: *An Evaluation of Wind Measurements by Four Doppler Sodars.* BAO Rep. No. 5, Wave Propagation Laboratory, NOAA/ERL, Boulder, CO, USA 110 pp.

Kristensen L. and Gaynor J.E., 1986: *Errors in Second Moments Estimated from Monostatic Doppler Sodar Winds. Part I: Theoretical Description.* J. Atmos. Oceanic Technol., Vol. 3, 523-528.

Kristensen L. and Gaynor J.E., 1986: *Errors in Second Moments Estimated from Monostatic Doppler Sodar Winds. Part II: Application to Field Measurement.* J. Atmos. Oceanic Technol., Vol. 3, 529-534.

Mahrt L, Heald R.C., Lenschow D.H., Stankov B.B. and Troen Ib, 1979: *An observational study of the structure of the nocturnal boundary layer.* Bound. Layer Meteorol., Vol. 17, 247-264.

Marsy E and Lui M.-C. G., 1976: *Discrete-Time Spectral Estimation of Continuous-Parameter Processes-A New Consistent Estimate.* IEEE Trans. Inf. Theory., IT-22, No. 3, 298-312.

Marsy E, 1978: *Alias-Free Sampling: An Alternative Conceptualization and its Applications.* IEEE Trans. Inf. Theory., IT-24, No. 3, 317-324.

Neave H.R., 1970:*Spectral analysis of a stationary time series using initially scarce data.* Biometrika, Vol 57, No. 1, 111-122.

Parzen E., 1962: *Spectral analysis of asymptotically stationary time series.* Bull. Int. Statist. Inst., 33rd Session, Paris.

Parzen E., 1963: *On spectral analysis with missing observations and amplitude modulation.* Sankhya, Vol. 25, Series A, 383-392.

Priestley M.B., 1981: *Spectral Analysis and Time Series,* volumes 1 and 2, Academic Press, New-York.

Scheinok P.A., 1965: *Spectral analysis with randomly missed observations: the binomial case.*Ann. Math. Statist., Vol. 36, 971-977.

Shiotani M. and Iwatani Y., 1976: *Horizontal Space Correlations of Velocity Fluctuations during Strong Winds.* J. Meteor. Soc. Japan, Vol. 54, No. 1, 59-66.

Srivastava R.C. and Atlas D., 1974: *Effect of Finite Radar Pulse Volume on Turbulence Measurements.* J. Appl. Meteor., Vol. 13, 472-480.

Thomas P. and Vogt S., 1990: *Measurement of wind data by Doppler-SODAR and tower instruments: An intercomparison.* Meteorol. Rdsch., Vol. 42, 161-165.

Underwood K.H., Coulter R.L., 1983: *Vertical Velocity Spectra from a Doppler sodar.* Proc. of the Second Int. Symp. Acous. Rem. Sensing of the Atmos. and Oceans, Rome, Italy.